Impairment of starvation-induced and constitutive autophagy in *Atg7*-deficient mice

Masaaki Komatsu,[1,3] Satoshi Waguri,[2] Takashi Ueno,[3] Junichi Iwata,[3] Shigeo Murata,[1] Isei Tanida,[3] Junji Ezaki,[3] Noboru Mizushima,[4] Yoshinori Ohsumi,[5] Yasuo Uchiyama,[2] Eiki Kominami,[3] Keiji Tanaka,[1] and Tomoki Chiba[1]

[1]Department of Molecular Oncology, Tokyo Metropolitan Institute of Medical Science, Bunkyo-ku, Tokyo 113-8613, Japan
[2]Department of Cell Biology and Neurosciences, Osaka University Graduate School of Medicine, Osaka 565-0871, Japan
[3]Department of Biochemistry, Juntendo University School of Medicine, Bunkyo-ku, Tokyo 113-8421, Japan
[4]Department of Bioregulation and Metabolism, Tokyo Metropolitan Institute of Medical Science, Bunkyo-ku, Tokyo 113-8613, Japan
[5]Department of Cell Biology, National Institute for Basic Biology, Okazaki 444-8585, Japan

Autophagy is a membrane-trafficking mechanism that delivers cytoplasmic constituents into the lysosome/vacuole for bulk protein degradation. This mechanism is involved in the preservation of nutrients under starvation condition as well as the normal turnover of cytoplasmic component. Aberrant autophagy has been reported in several neurodegenerative disorders, hepatitis, and myopathies. Here, we generated conditional knockout mice of *Atg7*, an essential gene for autophagy in yeast. *Atg7* was essential for ATG conjugation systems and autophagosome formation, amino acid supply in neonates, and starvation-induced bulk degradation of proteins and organelles in mice. Furthermore, *Atg7* deficiency led to multiple cellular abnormalities, such as appearance of concentric membranous structure and deformed mitochondria, and accumulation of ubiquitin-positive aggregates. Our results indicate the important role of autophagy in starvation response and the quality control of proteins and organelles in quiescent cells.

Introduction

There are two major protein degradation pathways in eukaryotic cells: the proteasome and the lysosome. The proteasome is a self-compartmentalized protease complex with catalytic activities inside its central proteinaceous chamber (Baumeister et al., 1998). It plays crucial roles in selective degradation of not only short-lived regulatory proteins but also abnormal proteins that should be eliminated from the cells (Goldberg, 2003). In contrast, the lysosome is a vesicle that contains many hydrolases, which are separated from the cytosol by the limiting membrane. In this lysosomal pathway, degradation of plasma membrane proteins and extracellular proteins is mediated by endocytosis, whereas degradation of cytoplasmic components is achieved through several pathways: macroautophagy, microautophagy, and chaperone-mediated autophagy (Seglen and Bohley, 1992; Dunn, 1994; Klionsky and Emr, 2000; Massey et al., 2004).

Macroautophagy (hereafter referred to as autophagy) is the main route for sequestration of the cytoplasm into the lysosome. The initial step of autophagy is elongation of the isolation membrane. The isolation membrane initially enwraps cytoplasmic constituents such as organelles, and then its edges fuse with each other forming a double membrane structure called autophagosome. Finally, the outer membrane of the autophagosome fuses with the lysosome/vacuole and the sequestered cytoplasmic components are degraded by the lysosomal/vacuolar hydrolases, together with the inner membrane of the autophagosomes (Mizushima et al., 2002).

In mammals, autophagy is considered necessary for the turnover of cellular components, particularly in response to starvation or glucagons (Mortimore and Poso, 1987). Yeast deficient in autophagy rapidly die under nutrition-poor conditions (Tsukada and Ohsumi, 1993), suggesting its important roles in preservation of nutrient supply. Indeed, autophagy is necessary for survival in early neonatal starvation period in mice (Kuma et al., 2004). Furthermore, autophagy plays a role in cellular remodeling during differentiation and development of multicellular organisms, such as fly, worm, and slime mold (Levine and Klionsky, 2004), and cellular defense against invading streptococcus (Nakagawa et al., 2004). Plants deficient in autophagy show accelerated senescence (Hanaoka et al., 2002). In humans, autophagy has been implicated in several pathological conditions (Shintani and Klionsky, 2004); e.g., low levels of autophagy were described in some malignant tumors (Liang et al., 1999).

Correspondence to Tomoki Chiba: tchiba@rinshoken.or.jp

Abbreviations used in this paper: MEF, mouse embryonic fibroblast; pIpC, polyinosinic acid–polycytidylic acid; PNS, postnuclear supernatant; SDH, succinate dehydrogenase.

The online version of this article includes supplemental material.

© The Rockefeller University Press $8.00
The Journal of Cell Biology, Vol. 169, No. 3, May 9, 2005 425–434
http://www.jcb.org/cgi/doi/10.1083/jcb.200412022

Supplemental Material can be found at:
http://www.jcb.org/cgi/content/full/jcb.200412022/DC1

In contrast, elevated levels of autophagosome formation were reported in other human pathologies such as neurodegenerative diseases, myopathies, and liver injury (Mizushima et al., 2002; Perlmutter, 2002), and autophagy is implicated in the execution of cell death (Xue et al., 1999; Bursch, 2001). However, the high level of autophagosome formation does not necessarily reflect enhanced protein degradation because the formation of autophagosomes is increased in Danon cardiomyopathy, which is characterized by defective lysosomal degradation (Nishino et al., 2000; Tanaka et al., 2000). Thus, it is not clear whether increased levels of autophagosome formation reflect the activation or defective protein degradation.

Although autophagy has been extensively studied, little was known about its molecular mechanism until the recent discovery of *ATG* genes in budding yeast (Tsukada and Ohsumi, 1993). Of the many *ATG* genes, seven uniquely compose two ubiquitin-like conjugation systems: ATG12 and ATG8 conjugation systems (Mizushima et al., 1998; Ichimura et al., 2000; Ohsumi, 2001). The ubiquitin-like protein Atg12p covalently attaches to Atg5p in a reaction similar to ubiquitination. In this process, Atg12p is activated by an E1-like enzyme, Atg7p (Tanida et al., 1999), and transferred to an E2-like enzyme, Atg10p (Shintani et al., 1999), and then finally conjugates to Atg5p. Atg8p, another ubiquitin-like protein, is unique among other ubiquitin-like molecules, as it conjugates to phosphatidyl-ethanolamine (Ichimura et al., 2000). Atg8p is activated by Atg7p, which is common to the Atg12 conjugation system, and is transferred to Atg3p, an E2-like enzyme (Ichimura et al., 2000). In mammals, there exist at least three Atg8 homologues that can all be activated by Atg7 (Tanida et al., 2001), GATE-16, GABARAP, and LC3 (Ohsumi, 2001), and they localize to the autophagosome (Kabeya et al., 2000, 2004).

Here, we generated conditional knockout mice of *Atg7* and analyzed the roles of autophagy in neonates and adult liver. Autophagosome formation and starvation-induced degradation of proteins and organelles was impaired in *Atg7*-deficient mice and adult livers. We also found an important role for autophagy in constitutive turnover of cytoplasmic components, and its loss resulted in accumulation of abnormal organelles and ubiquitinated proteins. Our results suggest that autophagy is important for clearance of ubiquitin-positive aggregates.

Results

Generation of Atg7 conditional knockout mice

To investigate the physiological roles of autophagy in mammals, we generated *Atg7* conditional knockout mice. Mouse *Atg7* gene is encoded by 17 exons that span 216-kb long genomic DNA. The active site cysteine residue essential for activation of the substrates is encoded by exon 14 and the targeting vector is designed to conditionally disrupt this exon by Cre-*loxP* technology. The targeted exon 14 was modified so that it could express Atg7 even in the presence of neo-resistant gene cassette in intron 14 (Fig. 1 A). Mice homozygous for the $Atg7^{Flox}$ allele (referred to as $Atg7^{F/F}$ mice), which were expected to express intact Atg7, were born healthy and fertile without any noticeable pathological phenotypes. Fig. 1 B shows Southern blots of mice with the indicated genotypes. Immunoblot analysis revealed the presence of Atg7 protein in $Atg7^{F/F}$ mouse embryonic fibroblasts (MEFs; Fig. 1 C), suggesting that Atg7 is efficiently expressed from the $Atg7^{Flox}$ allele.

The phenotype of Atg7-deficient mice

To examine the *Atg7*-deficient phenotype, we bred $Atg7^{F/F}$ mice with a line of transgenic mice that express the Cre recombinase under the control of the Zp3 promoter in the oocyte (Lewandoski et al., 1997). The heterozygous mice (referred to as $Atg7^{+/-}$) were obtained from female $Atg7^{F/+}$:Zp3 mice. $Atg7^{+/-}$ mice were born healthy and fertile without any noticeable pathological phenotypes for 1 yr. The $Atg7^{-/-}$ mice, obtained by breeding $Atg7^{+/-}$ mice, were born at Mendelian frequency (+/+: +/−: −/− = 21: 38: 19). The results of PCR genotyping are shown in Fig. 2 A. Neither Atg7 mRNA nor protein was detected in the homozygous mice (Fig. 2, B and C). We also tested the loss of Atg7 activity by examining the ATG conjugation systems in the neonate liver. A 56-kD protein, equivalent to Atg5–Atg12 conjugate, was detected by Atg5 antibody in the control $Atg7^{+/-}$ but not $Atg7^{-/-}$ liver (Fig. 2 C). In contrast, free Atg5 of 30 kD, which was faintly observed in the $Atg7^{+/-}$ liver, increased in $Atg7^{-/-}$ liver (Fig. 2 C). Mammalian Atg8p homologue LC3 has two forms (i.e., LC3-I and LC3-II; Kabeya et al., 2000). It is generally accepted that LC3-I is the free mature form whereas LC3-II is the lipidated form, in analogy to yeast Atg8p (Ichimura et al., 2000; Kabeya et al., 2000). Both forms were detected in $Atg7^{+/-}$ liver whereas only the LC3-I form was detected and increased in $Atg7^{-/-}$ liver (Fig. 2 C). When crossed with GFP-LC3 transgenic mice (Mizushima et al., 2004), the punctate structures representing autophagosomes were detected in $Atg7^{+/-}$ but not in $Atg7^{-/-}$ heart (Fig. 2, D and E). These results indicate that *Atg7* is essential for ATG conjugation systems and autophagosome formation in mice.

Although homozygous mice seemed normal at birth (Fig. 2 F) and had no apparent developmental defect by histological analyses (Fig. S1, available at http://www.jcb.org/cgi/content/full/jcb.200412022/DC1), the mean body weight of $Atg7^{-/-}$ mice (0.983 ± 0.0763 g, ± SD, $n = 9$) was significantly lower than that of wild-type and heterozygote mice (1.20 ± 0.116 g, $n = 29$; $P < 0.01$), and $Atg7^{-/-}$ mice died within 1 d after birth ($n = 19$). We considered that $Atg7^{-/-}$ mice could survive in utero by virtue of the nutrients supplied through the placenta but could not survive when the supply terminates after birth, as recently reported (Kuma et al., 2004). We tested the survival time of $Atg7^{-/-}$ neonates under starvation condition after caesarean delivery. Wild-type and heterozygous mice died at 21.7 ± 3.3 h after birth, whereas $Atg7^{-/-}$ mice died at 13 ± 2.0 h ($P < 0.01$; Fig. 2 G). To further test whether the cause of earlier death correlates with lower nutrient supply, we measured amino acid concentrations in plasma at 10 h after caesarean delivery. Essential and branched-chain amino acid concentrations in the sera of $Atg7^{-/-}$ mice were lower than those of wild-type mice (essential amino acids: 1.536 ± 0.087 vs. 1.291 ± 0.166 mmol/L, $P < 0.05$; branched-chain amino acids: 0.375 ± 0.038 vs. 0.268 ± 0.015 mmol/L, $P < 0.01$, respectively). The same

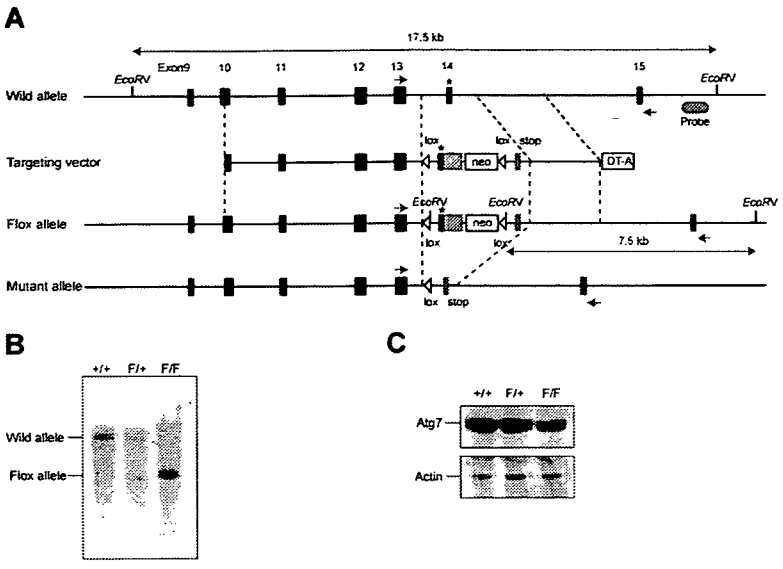

Figure 1. **Generation of *Atg7*$^{F/F}$ mice.** (A) Schematic representation of the targeting vector and the targeted allele of *Atg7* gene. The coding exons numbered in accordance with the initiation site as exon 1 are depicted by black boxes. Green and red boxes indicate *Atg7* cDNA fragment (aa 1786–2097) and *Atg7* cDNA fragment (aa 1669–1698) with stop codon, respectively. The open triangles denote *loxP* sequence. A probe for Southern blot analysis is shown as a gray ellipse. Arrows indicate the positions of PCR primers. The asterisk denotes the essential cysteine residue on exon 14. EcoRV, EcoRV sites; neo, neomycin-resistant gene cassette; DT-A, diphtheria toxin gene. (B) Southern blot analysis of genomic DNAs extracted from mice tails. Wild-type and Flox alleles are detected as 17.5- and 7.5-kb bands, respectively. (C) Immunoblot of Atg7 in MEFs. The lysates of MEFs of indicated genotypes were immunoblotted with Atg7 and actin.

results were also obtained using MEF cells from *Atg7*$^{-/-}$ mice (unpublished data). Together, these results indicate that *Atg7* is crucial for the recycling of amino acids in cells and survival of newborn mice under starvation condition.

Starvation response in adult mice liver

To delete *Atg7* gene in the adult mice, we bred the *Atg7*$^{F/F}$ mice with Mx1-Cre transgenic mice that express the Cre recombinase in response to interferon γ or its chemical inducer, polyinosinic acid–polycytidylic acid (pIpC). The Mx1-Cre transgenic mice can excise Flox allele completely in the liver and spleen and partially in the kidney and heart (Kuhn et al., 1995). Intraperitoneal injections of pIpC resulted in effective recombination of the *Atg7*^{Flox} allele in the liver and spleen (Fig. S2, available at http://www.jcb.org/cgi/content/full/jcb.200412022/DC1; and not depicted). No Atg7 transcript, protein, and activity were detected, similar to *Atg7*$^{-/-}$ mice (Fig. S2). Next, we tested the autophagosome formation under fasting condition. 1-d fasting resulted in induction of typical autophagosomes in control *Atg7*$^{F/+}$:Mx1 mice (Fig. 3, A–D and I). In contrast, no such induction of autophagosome formation was noted in the liver of fasted *Atg7*$^{F/F}$:Mx1 mice (Fig. 3, E, F, and I). Although some autophagosome-like structures were occasionally observed both in fed and fasted mutant mice livers (Fig. 3, G and H), they

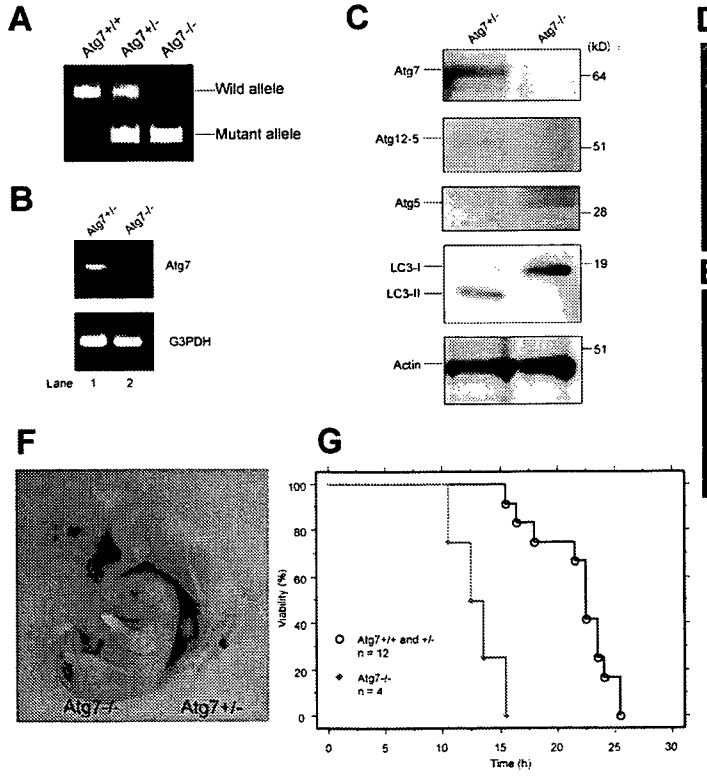

Figure 2. **The phenotypes of *Atg7*-deficient mice.** (A) PCR analysis of genomic DNA extracted from wild-type, *Atg7*$^{+/-}$, and *Atg7*$^{-/-}$ mice tail. The amplified fragments derived from wild and mutant alleles are indicated. (B) Expression of Atg7 transcript. Atg7 transcript was detected by RT-PCR analysis. The region amplified was between exons 12 and 13. G3PDH cDNA was amplified as an internal control. (C) ATG conjugation systems in *Atg7*$^{-/-}$ mice liver. The liver homogenate was centrifuged at 800 *g* for 10 min and the postnuclear supernatant (PNS) was immunoblotted with antibodies against Atg7, Atg5, LC3, and actin as a loading control. The bottom panel of Atg5 blotting is the long exposure of the top panel to detect free Atg5. Data shown are representative of three separate experiments. (D and E) Deficiency of autophagosome formation in *Atg7*$^{-/-}$ heart. *Atg7*$^{+/-}$ (D) and *Atg7*$^{-/-}$ (E) mice expressing GFP-LC3 were obtained by caesarean delivery and analyzed by fluorescence microscopy. Representative results obtained from each neonatal heart at 3 h after caesarean delivery. (F) Morphology of *Atg7*$^{+/-}$ and *Atg7*$^{-/-}$ mice. (G) Kaplan-Meier curves of survival of newborn mice. Control and *Atg7*$^{-/-}$ mice were delivered by caesarean section, and their survival was followed up to 26 h.

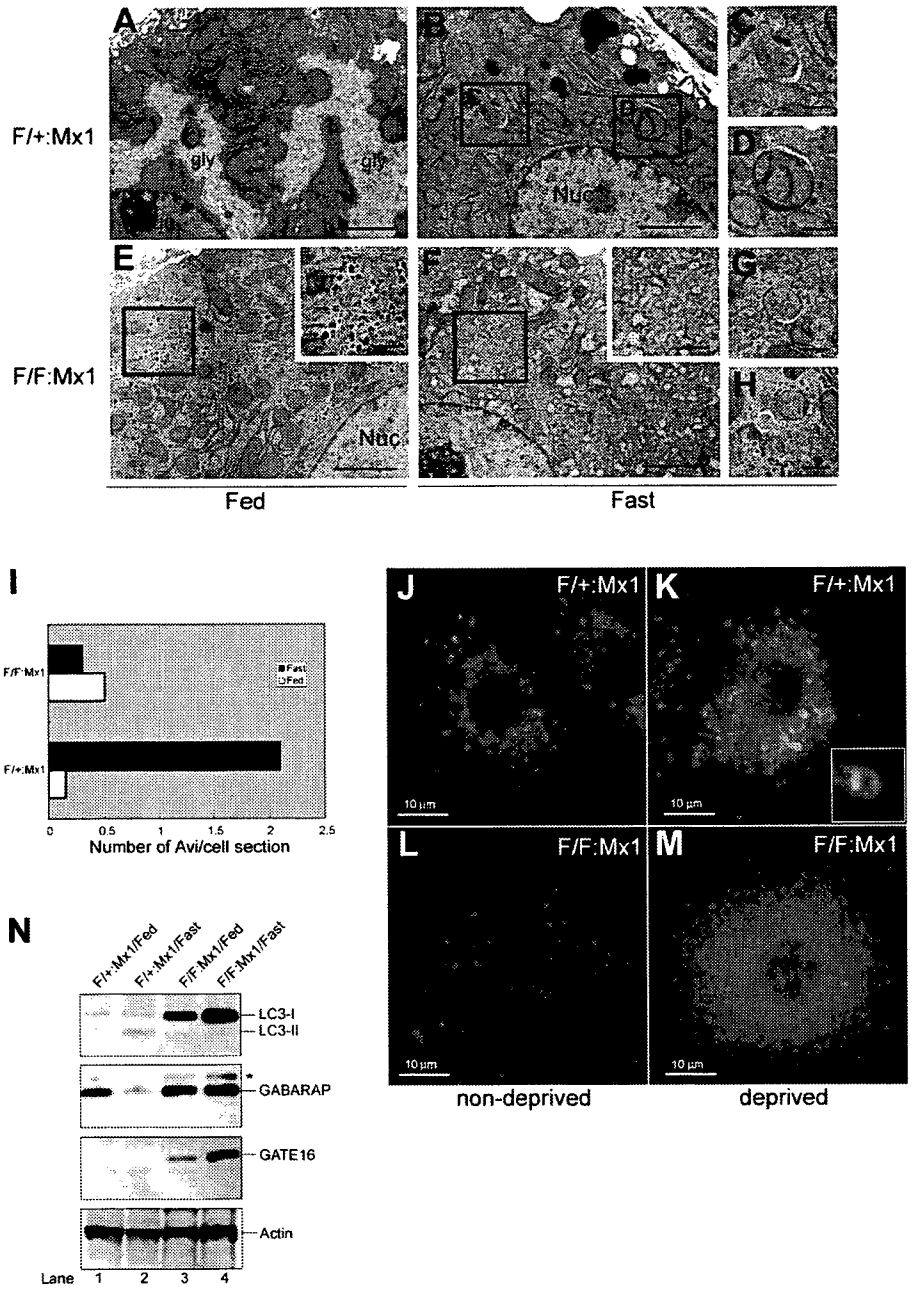

Figure 3. **Impaired autophagosome formation in *Atg7*-deficient liver.** (A–H) Electron micrographs of liver from $Atg7^{f/+}$:Mx1 (A–D) and $Atg7^{F/F}$:Mx1 (E–H) mice fed ad libitum (A and E) or fasted for 1 d (B and F). (C and D) Early stages of autophagic vacuoles observed in B are highlighted. (E and F) Autophagosome was not induced in mutant hepatocytes upon fasting. Insets show higher magnification views of glycogen granules. (G and H) Occasionally observed autophagosome-like structures in mutant hepatocytes. Bars: (A, B, E, and F) 5 μm; (C, D, G, and H) 0.5 μm. (I) Number of autophagosomes per hepatocyte (n = 20) in each genotype was counted and their averages are shown. (J–M) Immunofluorescent analysis of LC3 in primary cultured hepatocytes. Hepatocytes isolated from $Atg7^{f/+}$:Mx1 (J and K) and $Atg7^{f/F}$:Mx1 (L and M) were cultured in Williams' E (J and L) or Hanks' solution (K and M). Inset highlights the cup-like structure of LC3 observed in K. (N) Immunoblot analysis of Atg8 homologues in the liver. $Atg7^{f/+}$:Mx1 (lanes 1 and 2) and $Atg7^{f/F}$:Mx1 mice (lanes 3 and 4) were fed ad libitum (lanes 1 and 3) or fasted for 1 d (lanes 2 and 4), and then PNS fractions of liver were analyzed by immunoblotting with anti-LC3, GABARAP, GATE-16, and actin antibodies. Asterisk denotes a nonspecific band. Data shown are representative of three separate experiments.

tended to be smaller than those observed in fasted control liver and hardly contained large cytoplasmic organelles (compare with Fig. 3, C and D). The number of autophagosomes per hepatocyte was counted and the mean values are shown in Fig. 3 I. The mutant hepatocytes lacked typical glycogen area, in contrast to the fed hepatocytes (Fig. 3, A and E); however, well-developed glycogen granules (α granules) were observed between numerous smooth endoplasmic reticula (Fig. 3 E, inset). Immunofluorescent analysis also revealed the presence of many cup-shaped and ringlike structures representing autophagosomes in the control hepatocytes (Fig. 3, J and K). Although several LC3-positive dots were observed in the mutant hepatocytes, they were not induced in response to starvation and did not form cup-shaped and ringlike structures (Fig. 3, L and M).

Next, we examined the fasting response of LC3 and other homologues, GABARAP and GATE-16, by immunoblotting (Fig. 3 N). LC3 is known to be up-regulated and recruited to the autophagosome upon starvation and degraded in the lysosomes (Kabeya et al., 2000). Fasting slightly increased the modification of LC3 in heterozygous liver. In the mutant liver, no modification of LC3 was noted and LC3-I increased in response to fasting. These results suggest that LC3 is up-regulated, but its modification and degradation are impaired in mutant mice. The level of GABARAP did not change upon fasting in the mutant liver, whereas it decreased in the heterozygous liver, suggesting that GABARAP is not up-regulated but its degradation after modification is impaired in mutant liver. Although GATE-16 was hardly detected in the heterozygous liver under both fed and fasting conditions, it was clearly detected

and increased upon fasting in the mutant liver. These results suggest that GATE-16 may be constitutively degraded even at fed condition in heterozygous mice and up-regulated in response to fasting under defective *Atg7*. The levels of all LC3 homologues were elevated even at fed condition in the mutant liver, suggesting their marked stabilization in autophagy-deficient condition. However, the possibility that their transcriptions are up-regulated at basal level due to *Atg7* deficiency cannot be excluded. We sought to determine their localizations in the cells. However, our antibodies for these molecules were not applicable for immunofluorescent analyses, and those localizations remain to be clarified. In conclusion, all Atg8 homologues respond to fasting, although in a different manner, and their levels are affected by the absence of Atg7.

Atg7 is indispensable for fasting-induced degradation of cytosolic proteins and organelles in the mouse liver

Given that autophagosome formation was impaired in *Atg7*-deficient liver, we next examined its effects on the bulk degradation of proteins and organelles under fasting condition. After 1-d fasting in control $Atg7^{F/+}$:Mx1 and mutant $Atg7^{F/F}$:Mx1 mice, the liver was dissected and the amount of total protein per whole liver was measured. The amount of total liver proteins decreased to ~66% by 1-d fasting in the control liver (Fig. 4 A). In contrast, fasting did not significantly decrease the amount of total liver proteins in the mutant liver. Moreover, the amount of total proteins in the mutant liver was 1.5-fold that of control. These results indicate that the decrease of total proteins is dependent on Atg7 and autophagosome formation.

We also examined whether or not fasting causes the degradation of cellular organelles such as mitochondria in the livers of mice. To quantify the amount of the mitochondria, we first measured the activity of mitochondrial enzyme succinate dehydrogenase (SDH) in total liver extracts. In the control livers, fasting was associated with a significant decrease of SDH activity, and the reduction was proportional with the decrease in the amount of total protein (Fig. 4 B). In contrast, fasting was not associated with any change in SDH activity in the mutant livers. Similar to total protein, the basal SDH activity in mutant liver was significantly higher than in control. The effect of fasting on the amount of the mitochondria was also assessed by immunoblot analysis of mitochondrial protein cytochrome *c* (Fig. 4 C). When equal amounts of proteins were loaded, the level of cytochrome *c* was equivalent in the two genotypes at either fed or fasting conditions, suggesting that the ratio of mitochondria versus total protein is not altered by fasting in both genotypes. Considering that the total protein amounts decreased by fasting in the control liver (Fig. 4 A), these results suggest that the mitochondria and cytoplasmic proteins are proportionally degraded upon fasting in heterozygous mice. However, such degradation is impaired in *Atg7*-deficient liver because the levels of both proteins and mitochondria are unchanged and kept at a higher level.

Next, we investigated the effect of autophagy deficiency on protein turnover. To quantify the turnover of long-lived protein, after each control and mutant hepatocytes had been labeled with [^{14}C]leucine for 24 h and chased for 2 h, the release of TCA-soluble [^{14}C]leucine was measured for 4 h. In control hepatocytes, nutrient deprivation significantly induced protein degradation, and such degradation was suppressed by the addition of lysosomal inhibitors such as monomethylamine and E64d and pepstatin (Fig. 4 D). The induced degradation was still observed in the presence of proteasome inhibitor epoxomicin, suggesting that such protein degradation is mediated in the lysosomal pathway rather than the proteasome (Fig. 4 D). In the mutant hepatocytes, degradation of long-lived protein was not induced by nutrient deprivation (Fig. 4 D), indicating that autophagy is the main route for lysosomal degradation under starvation condition. Consistent with these results, amino acid concentrations in starved mutant hepatocytes were lower than in control hepatocytes (unpublished data). Intriguingly, although lysosomal inhibitors inhibited protein degradation even

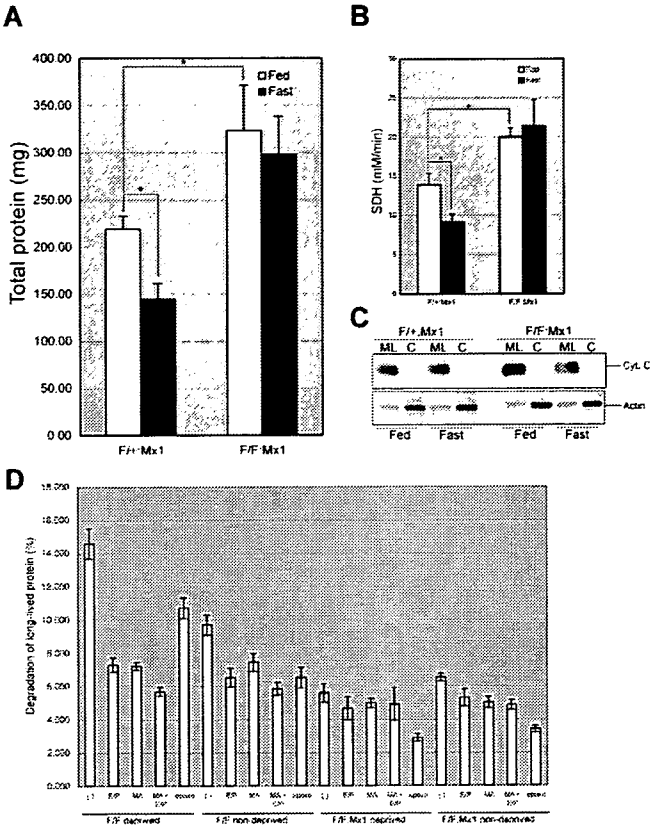

Figure 4. **Fasting response of *Atg7*-deficient liver.** (A and B) Livers from $Atg7^{F/+}$:Mx1 and $Atg7^{F/F}$:Mx1 mice fed ad libitum (Fed) or fasted for 1 d (Fast) at 20 d after pIpC injection were dissected, and the amount of total protein (A) and SDH activity (B) per liver were measured. Data are mean ± SD values of five mice in each group; *, $P < 0.01$. (C) Cytochrome *c* levels in the cytosolic and mitochondria/lysosomal fractions of the liver at 20 d after injection. Equal amount of PNS fractions were centrifuged at 8,000 *g* for 10 min and the pellets were used as the mitochondrial/lysosomal fraction (ML). The supernatants were further centrifuged at 100,000 *g* for 1 h and the supernatant was used as the cytosolic fraction (C). Actin was blotted as control. Data shown are representative of two separate experiments. (D) Turnover of long-lived protein. Hepatocytes from $Atg7^{F/+}$:Mx1 and $Atg7^{F/F}$:Mx1 mice were isolated and labeled with [^{14}C]leucine for 24 h, and degradation of long-lived protein in deprived or nondeprived condition was measured. Monomethylamine (MA) and/or E64d and pepstatin (E/P) or epoxomicin (epoxo) was added as indicated. Data are the mean ± SD of triplicate experiments.

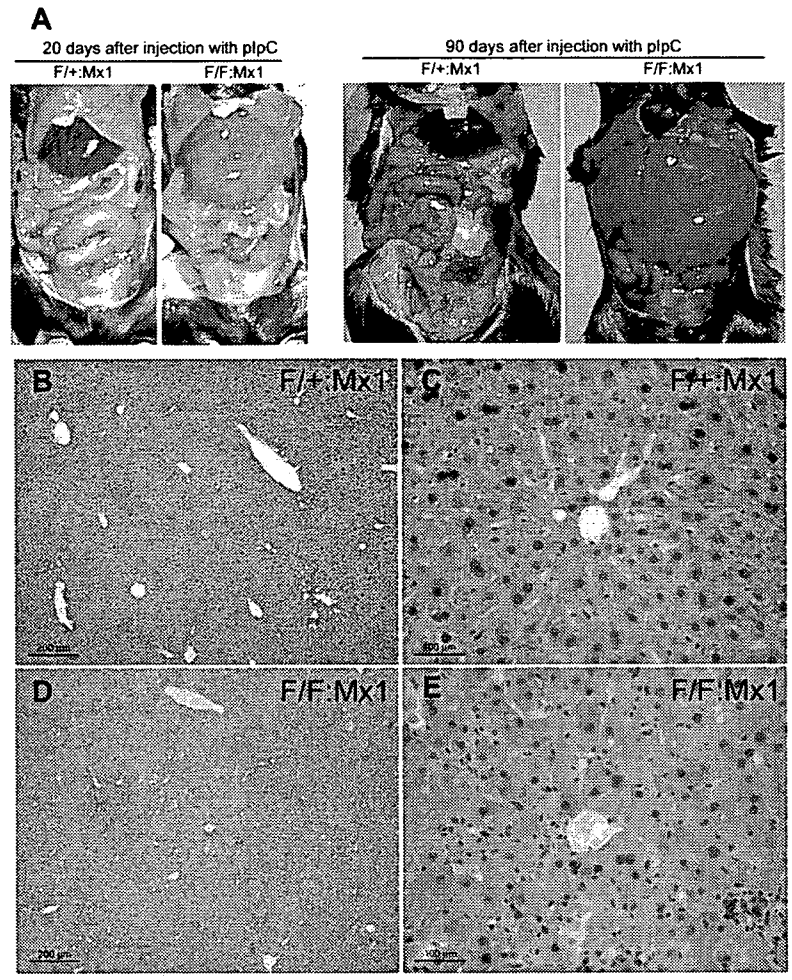

Figure 5. ***Atg7* deficiency in the liver causes hepatomegaly and hepatic cell swelling.** (A) The gross anatomical views of representative mice at the indicated day after pIpC injection. (B–E) Histology of representative livers with *Atg7* deficiency. Hematoxylin and eosin staining of $Atg7^{F/+}$:Mx1 (B and C) and $Atg7^{F/F}$:Mx1 (D and E) liver at 90 d after pIpC injection.

at nondeprived condition in the control hepatocytes, such inhibition was not significant in the mutant hepatocytes (Fig. 4 D), indicating that significant amounts of proteins are constitutively degraded in the lysosome via autophagic pathway. Together, these results suggest that autophagy plays a significant role in turnover of long-lived protein.

Loss of *Atg7* in the liver leads to hepatomegaly and accumulation of abnormal organelles in hepatic cells

We further chased the phenotypes of the mutant mice for up to 90 d after pIpC injection. Gross anatomy revealed severe enlargement of the liver, filling up most of the abdominal cavity (Fig. 5 A). Other major organs were normal histologically (Fig. S3, available at http://www.jcb.org/cgi/content/full/jcb.200412022/DC1). The mean liver weights of control and mutant mice at 90 d after pIpC injection were 1.39 ± 0.24 and 6.10 ± 2.06 g, respectively (n = 5 each). Histological analysis revealed disorganized hepatic lobules and cell swelling in the mutant liver (Fig. 5, D and E). No hepatocellular proliferation or regeneration was detected (unpublished data). Vacuolated hepatic cells were occasionally observed and those were associated with hepatic cell death, which is consistent with the leakage of alkaline phosphatase, aspartate aminotransferase, and alanine aminotransferase in the mutant mice sera (Fig. S4, available at http://www.jcb.org/cgi/content/full/jcb.200412022/DC1).

Although most hepatocytes were still alive in the mutant liver, ultrastructural analysis revealed the appearance of aberrant concentric membranous structures (Fig. 6, A and B), which were also observed as early as 20 d after pIpC-injected liver (not depicted). These structures surrounded various cytoplasmic constituents such as mitochondria, lipid droplets, and vesicular structures (Fig. 6 A). Their membranous elements were continuous with the rough ER (Fig. 6 B, arrowheads), and the corresponding structures were positive for calreticulin, an ER protein marker (not depicted), indicating that these structures originated from the rough ER. Accumulation of peroxisomes (Fig. 6 C) and deformed mitochondria (Fig. 6, C and D) was also observed in the mutant liver. These results suggest the important role of autophagy in turnover of organelles, and its defect results in accumulation of abnormal organelles.

Formation of ubiquitin-positive inclusions in *Atg7*-deficient hepatocytes

Autophagy has been implicated in not only organelle turnover but also in elimination of protein aggregates (Kopito, 2000). Protein aggregates are often ubiquitinated. In the next step, we immunostained the liver with an ubiquitin antibody to examine the presence of such aggregates. Several ubiquitin-positive par-

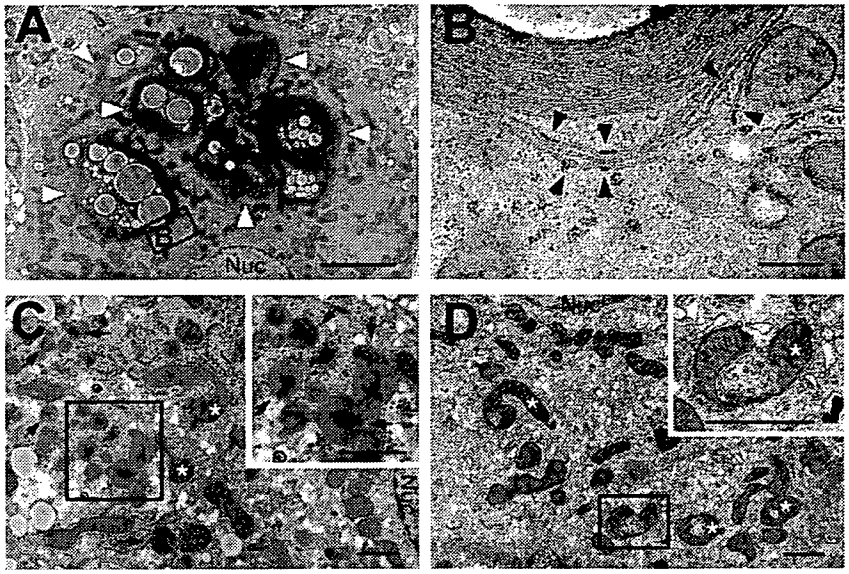

Figure 6. **Electron micrographs of hepatic cells with *Atg7* deficiency.** (A and B) Note the presence of concentric membranous structures in the mutant cells (arrowheads). Higher magnification view (B) shows the membranous elements are continuous with the rough ER (arrowheads). (C and D) The mutant cells contained a high number of peroxisomes (arrows) and deformed mitochondria (asterisks). Insets show higher magnification views. Nuc, nucleus. Bars: (A) 5 μm; (B) 0.5 μm; (C and D) 1 μm.

ticles of various sizes were detected in the $Atg7^{F/F}$:Mx1 but not in $Atg7^{F/+}$:Mx1 hepatic cells at both 10 and 90 d after pIpC injection (Fig. 7, A and B; and Fig. S5, available at http://www.jcb.org/cgi/content/full/jcb.200412022/DC1). The immunoblots of the liver lysates revealed the accumulation of high-molecular mass polyubiquitinated proteins in the mutant liver (Fig. 7 G and Fig. S5), suggesting that the ubiquitin particles are aggregates of polyubiquitinated proteins. To further determine the localization of ubiquitin-positive dots, analysis of immunoelectron micrographs was performed. Numerous particles of colloidal gold, indicative of ubiquitin, were detected on lipid dropletlike structures, membranous structures, and amorphous substances in the cytoplasm (Fig. 7, C–F). Such signals were not observed in the wild-type liver (unpublished data).

The accumulation of ubiquitin-positive inclusions in the cytoplasm prompted us to examine the effect of autophagy deficiency on proteasome function. Immunoblots of proteasome subunits (p112/Rpn2, Mss1/Rpt1, and α5) showed that their relative amounts were not affected in the mutant liver (Fig. 7 G). Furthermore, the activities of the proteasome, measured by Suc-LLVY-MCA as substrate, were also comparable between wild-type and mutant livers (unpublished data). These results indicate the accumulation of ubiquitin-positive aggregates in autophagy-deficient hepatocytes despite the apparently normal proteasome function.

Discussion

Autophagy is a bulk protein degradation pathway, which is conserved in eukaryotes, essential for the survival of unicellular organisms under nutrient-poor condition and for cellular remodeling of multicellular organisms (Mizushima et al., 2002; Levine and Klionsky, 2004). In the present study, we generated conditional knockout mice of *Atg7* gene, which is an essential gene for autophagy in budding yeast, and analyzed its roles in mice.

In mammals, *Atg7* was indeed essential for ATG12 conjugation, LC3 modification systems, and autophagosome formation (Fig. 2, Fig. 3, and Fig. S2). Immunofluorescent analyses revealed that LC3-positive dots appeared but did not form cup-shaped and ringlike structures in $Atg7^{F/F}$:Mx1 livers (Fig. 3). The LC3-I form is usually present at the S100 fraction and the LC3-II form at the P100 fraction (Kabeya et al., 2000). In the mutant liver, LC3-I was present in both S100 and P100 fractions (unpublished data), suggesting that the LC3-positive dots in the mutant hepatocytes are indeed the LC3-I form. These results suggest that LC3 may be recruited to the dot structures independent of the modification (Fig. 3). In mammals, LC3 has at least two homologues, GABARAP and GATE-16, which share common biochemical characteristics (Tanida et al., 2001) and localize to autophagosome in response to fasting (Kabeya et al., 2004). Indeed, the modification and levels of these molecules under fasting condition were affected in the mutant liver (Fig. 3 N). However, these LC3 homologues have been identified in a different biological pathway and may have diverse functions (Ohsumi, 2001). Thus, how their functions and localizations are affected in *Atg7*-deficient cells remains to be clarified.

Although $Atg7^{-/-}$ mice were born at Mendelian ratio, and the major organs were almost normal histologically (Fig. S1), they had reduced body weight and died within 1 d after birth. $Atg7^{-/-}$ mice had lower amino acid level and died earlier compared with wild type under nonsuckling condition after caesarean delivery (Fig. 2 G), suggesting that *Atg7* is important for survival during the early neonatal starvation period, similar to recently reported $Atg5^{-/-}$ mice phenotypes (Kuma et al., 2004). However, because suckling $Atg7^{-/-}$ mice also died within 1 d after birth (unpublished data), the cause of death may not be only due to low level of amino acids. The reason for the reduced body size is also unclear and may be related to placental function or due to inefficient reutilization of nutrients during embryogenesis. It is of note that a lower level of autophagy occurs during embryogenesis (Mizushima et al., 2004) even when nutrients are supplied from the placenta. Furthermore, *Atg7* null mice possess several ubiquitin-positive inclusions in some

organs at the time of birth (unpublished data). This phenotype might be related to the earlier death of mutant. Further analysis of $Atg7^{-/-}$ mice is required to unravel the roles of autophagy, and such analysis is currently under way by breeding the $Atg7^{F/F}$ mice with several Cre-transgenic mice.

Starvation-induced autophagosomes appeared to sequester the cytoplasm randomly (Fig. 3). Consistent with this notion, the amount of mitochondria decreased in proportion with reduction in the amount of total protein (Fig. 4, A–C). These results suggest that mitochondria are degraded nonselectively under fasting condition. In *Atg7*-deficient liver, no autophagosome formation was noted and the degradation of proteins and organelles under fasting condition was largely impaired. These results suggest that the rapid reduction of proteins and organelles upon fasting is dependent on *Atg7* and autophagosome formation.

Although autophagy can be induced by starvation, this pathway may take place even at feeding condition at basal level. This constitutive pathway may be important for turnover of organelles and cytoplasmic proteins. Indeed, the degradation of long-lived protein was inhibited in mutant hepatocytes irrespective of nutrient deprivation (Fig. 4 D), and multiple abnormalities of organelles (e.g., the presence of concentric membranous structure and accumulation of deformed mitochondria) were observed in *Atg7*-deficient hepatocytes (Fig. 6). Unexpectedly, the morphologically abnormal mitochondria appear to retain their function, as judged by the normal membrane potentials and the absence of cytochrome *c* leakage in the cytosol (unpublished data). In contrast to starvation-induced autophagy, whether or not constitutive autophagy eliminates abnormal and excess organelles in a degree of selectivity remains to be clarified.

Beclin 1, a human homologue of *ATG6/VPS30* essential for autophagy in yeast, was recently identified as a tumor suppressor gene, and autophagy has been implicated in the regulation of cellular proliferation (Liang et al., 1999). Indeed, heterozygous disruption of mouse *Beclin 1* led to enhanced tumorigenesis (Qu et al., 2003; Yue et al., 2003). *Atg7* deficiency led to hepatomegaly (Fig. 5 A), suggesting that cell proliferation or malignant transformation might be induced in the *Atg7*-deficient cells.' However, neither tumorigenesis nor enhanced cell proliferation was detected as tested by BrdU incorporation at 90 d after pIpC injection in the mutant liver compared with control mice (unpublished data). The hepatomegaly observed in the mutant mice was likely due to increased cellular volume rather than cell number, which is also supported by the swollen appearance of hepatocytes (Fig. 5, D and E).

In *Atg7*-deficient liver, we detected numerous ubiquitin-positive particles indicative of protein aggregates (Fig. 7 and Fig. S5). It has been reported that proteasome inhibition leads to aggregate formation. Conversely, the formation of protein aggregates inhibits the proteasome (Bence et al., 2001), resulting in a malignant cycle of aggregate formation and proteasome inhibition. In the mutant liver, failure of the proteasome was postulated; however, no impairment of proteasome function, in terms of its expression or peptidase activities, was noted (Fig. 7 G and not depicted). Our results suggest that the ubiquitinated proteins eventually aggregate even in the presence of functional proteasomes. Considering that such ubiquitinated aggregates must be difficult to unfold, and proteasomes need to unfold their substrate before degradation (Baumeister et al., 1998), it is likely that elimination of ubiquitin-positive aggregates in the cells is largely dependent on the autophagic process. Protein ubiquitination may also occur after protein aggregation. In either case, we propose the possibility that protein ubiquitination may serve as a signal to the autophagic process in addition to the proteasomes pathway. In this context, it is worth noting that sperm mitochondria are known to be ubiquitinated before degradation during fertilization (Sutovsky et al., 1999). It is now well established that ubiquitin regulates not only proteasomal degradation, but also lysosomal degradation. Thus, it is conceivable that ubiquitin could also regulate the autophagic pathway.

A growing number of disease-associated proteins have been found to accumulate in aggresome, including huntingtin, parkin, α-synuclein, and peripheral myelin protein 22 (Notterpek et al., 1999; Ciechanover and Brundin, 2003). The aggregation of these proteins is thought to be involved in the pathogenesis of Huntington's disease, Parkinson's disease, and peripheral neu-

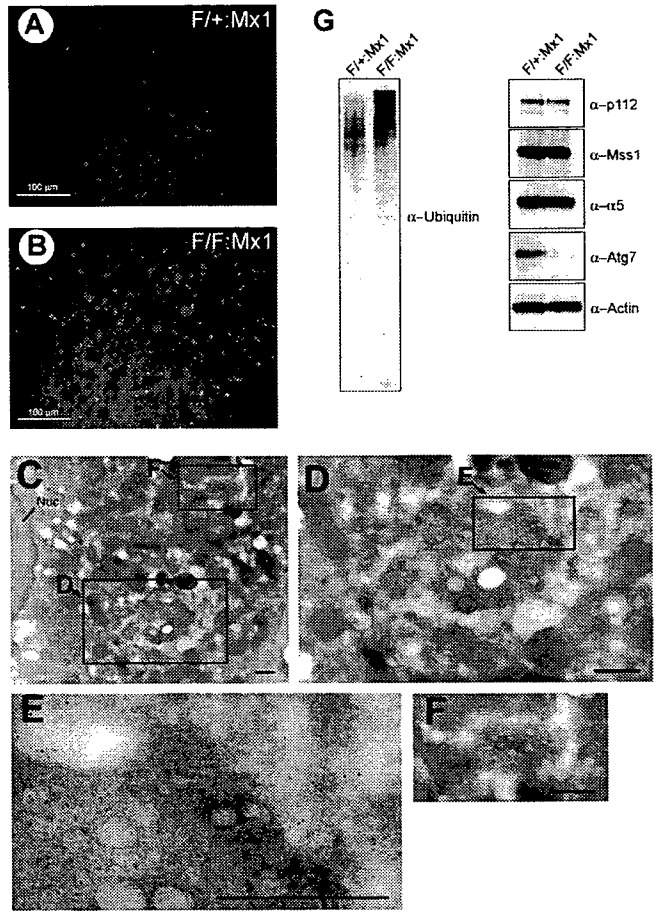

Figure 7. **Accumulation of ubiquitin-positive aggregates in *Atg7*-deficient liver.** (A and B) Immunofluorescent detection of ubiquitin in the $Atg7^{F/+}$:Mx1 (A) and $Atg7^{F/F}$:Mx1 (B) liver. (C–F) Immunoelectron micrographs of ubiquitin in a representative mutant liver. The high-magnification view shows ubiquitin particles near the lipid dropletlike structure (D–F). Bars, 0.5 μm. (G) Immunoblot analysis of the liver. PNS fractions of the liver at 90 d after injection were immunoblotted with the indicated antibodies. Data shown are representative of three separate experiments.

ropathies, respectively. Enhanced autophagosome formation is prevalent in most of these diseases (Mizushima et al., 2002), and autophagy has also been considered as a caspase-independent cell death pathway (Xue et al., 1999; Bursch, 2001). Our *Atg7* mutant mice should be useful for examining the role of autophagy in the cell death pathway or in a cellular defense mechanism in the pathogenesis of these diseases.

Materials and methods

Generation of $Atg7^{f/F}$ mice

The targeting vector was constructed by insertion of a *loxP* sequences within introns 13 and 14 of *Atg7* gene. Exon 14 was fused to a cDNA fragment encoded by exons 15, 16, and 17 (aa 1786–2097) and polyA signal sequence was added after the stop codon. Neo resistant gene cassette (*mc1-neo-pA*) was ligated behind the polyA signal sequence followed by the second *loxP* sequence, splicing acceptor site, and exon 14 with stop codon preceding the active site. We electroporated the targeting vector into mouse TT2 ES cells, selected with 200 μg/ml G418 (GIBCO BRL), and then screened for homologous recombinants by PCR and Southern blot analyses. PCR primers were as follows: 5′-TGGCTGCTACTTCTGCAATGATGT-3′, 5′-GAAGGGACTGGCTGCTATTGGGCGAAGTGC-3′, and 5′-TTAGCACAGGGAACAGCGCTCATGG-3′. Southern blot analysis was performed by digestion of genomic DNA with EcoRV and hybridization with the probe shown in Fig. 1 A. Genotyping of mice by PCR was performed using the following two primers: 5′-TGGCTGCTACTTCTGCAATGATGT-3′ and 5′-CAGGACAGAGACCATCAGCTCCAC-3′. Progeny containing the $Atg7^{flox}$ allele were bred with *Zp3*-Cre and *Mx1*-Cre transgenic mice to produce $Atg7^{-/-}$ and $Atg7^{f/F}$:Mx1 mice, respectively. With regard to $Atg7^{f/F}$:Mx1 mice, Cre expression in the liver was induced by i.p. injection of pIpC (Sigma-Aldrich). 300 μl pIpC solution (1 mg/ml in water) was injected three times at 48-h intervals. Mice were housed in specific pathogen-free facilities, and the experimental protocol was approved by the Ethics Review Committee for Animal Experimentation of the Tokyo Metropolitan Institute of Medical Science.

RT-PCR analysis

cDNA was synthesized from 5 μg of DNase I–treated total RNA using the SuperScript First-Strand Synthesis System (GIBCO BRL) and oligo $(dT)_{12\text{-}18}$ primers. Specific primers for each gene were as follows: 5′-ATGCCAGGACACCCTGTGAACTTC-3′ and 5′-ACATCATTGCAGAAGTAGCAGCCA-3′ for Atg7, and 5′-GAGCTGAACGGGAAGCTCAC-3′ and 5′-ACCACCCTGTTGCTGTAGC-3′ for G3PDH.

Immunoblot analysis

The fractions were immunoblotted as described previously (Komatsu et al., 2001). The antibodies for Atg7 (Tanida et al., 1999) and Atg5 (Mizushima et al., 2001) were described previously. The antibodies for ubiquitin (DakoCytomation) and actin (MAB1501R; Chemicon International, Inc.) were purchased. The antibodies against LC3, GABARAP, and GATE-16 were raised in rabbits using their specific peptides as antigens. The antibodies against p112, Mss1, and α5 were provided by K.B. Hendil (August Krogh Institute, University of Copenhagen, Copenhagen, Denmark).

Caesarean delivery and measurement of amino acids

Newborns were delivered by caesarean section at 19.0 d postcoitus and placed in a humidified, thermostat-controlled chamber (30°C). Plasma was fixed in 3% sulphosalicylic acid. Amino acids in the supernatant from plasma samples were measured by an amino acid analyzer (L8500A; Hitachi).

Protein degradation assay

The assay was performed essentially as described previously (Gronostajski and Pardee, 1984). In brief, hepatocytes were plated at 5×10^4 cells/well in collagen-coated 24-well plates and cultured in Williams' E medium with 10% FCS (Williams' E/10% FCS) for 24 h. Cells were incubated with Williams' E/10% FCS containing 0.5 μCi/ml [^{14}C]leucine for 24 h to label long-lived proteins. Cells were washed with Williams' E/10% FCS containing 2 mM of unlabeled leucine and incubated with the medium for 2 h to allow degradation of short-lived proteins and minimize the incorporation of labeled leucine, which was released by proteolysis into protein. The cells were then washed with PBS and incubated at 37°C with Krebs-Ringer bicarbonate medium and Williams' E/10% FCS in the presence or absence of protease inhibitors (5 mM monomethylamine, 10 μg/ml E64d and pepstatin, or 5 μM epoxomicin). After 4 h, aliquots of the medium were taken and a one-tenth volume of 100% trichloroacetic acid was added to each aliquot. The mixtures were centrifuged at 12,000 *g* for 5 min, and the acid-soluble radioactivity was determined using a liquid scintillation counter. At the end of the experiment, the cultures were washed twice with PBS, and 1 ml of cold trichloroacetic acid was added to fix the cell proteins. The fixed cell monolayers were washed with trichloroacetic acid and dissolved in 1 ml of 1 N NaOH at 37°C. Radioactivity in an aliquot of 1 N NaOH was determined by liquid scintillation counting. The percentage of protein degradation was calculated according to published procedures (Gronostajski and Pardee, 1984).

Histological examination

Tissues were dissected, fixed in 4% PFA, paraffin embedded, and sectioned. Sections were stained by Meyer's hematoxylin and eosin. For immunohistochemical analysis, sections were blocked in 5% normal goat serum in PBS containing 0.2% Triton X-100, and then incubated with antiubiquitin antibody (1B3; MBL International Corporation) and Alexa 488–labeled secondary antibody (Molecular Probes). Apoptotic cells were detected by TUNEL assay using Apoptag kit (Intergen Company) as described previously (Tateishi et al., 2001). For GFP-LC3 observations, tissues were fixed with 4% PFA, and the cryosections were imaged with a conventional fluorescence microscope. For LC3 staining, hepatocytes were fixed and stained with anti-LC3 antibody as described previously (Kabeya et al., 2000). All fluorescence images were obtained using a fluorescence microscope (model Q550FV; Leica) equipped with cooled charge-coupled device camera (model CTR MIC; Leica). Pictures were taken using Qfluoro software (Leica).

EM and immunoelectron microscopy

Livers were fixed by cardiac perfusion using 0.1 M phosphate buffer containing 2% PFA and 2% glutaraldehyde for conventional EM. They were post-fixed with 1% OsO_4, embedded in Epon812, and sectioned. Immunoelectron microscopy was performed on cryothin sections as described previously (Waguri et al., 1995). In brief, livers were frozen in phosphate buffer with 2.3 M sucrose and 20% polyvinyl pyrrhoridon. Ultrathin sections were mounted on Formvar carbon-coated nickel grids, blocked with 1% BSA in PBS, and incubated with antiubiquitin antibody (1B3) and colloidal gold conjugated secondary antibody.

Other procedures

MEFs were prepared as described previously (Murata et al., 2001). Primary hepatocytes were prepared as described previously (Ueno et al., 1990). Cell starvation was conducted by incubating the cells in Hanks' balanced solution after three separate washes. The SDH activity was assayed as described previously (Ueno et al., 1990).

On line supplemental material

Fig. S1 shows the histological analyses of tissues from $Atg7^{+/-}$ and $Atg7^{-/-}$ mice at 1 d after birth. Fig. S2 shows the loss of Atg7 protein and activity in $Atg7^{f/F}$:Mx1 mouse liver. Fig. S3 shows the histological analyses of tissues from $Atg7^{f/+}$:Mx1 and $Atg7^{f/F}$:Mx1 mice. Fig. S4 shows the cell death in autophagy-deficient liver. Fig. S5 shows the accumulation of ubiquitin-positive inclusions at early stage of autophagy deficiency. Further comments on the data can be found in the legends. Online supplemental material is available at http://www.jcb.org/cgi/content/full/jcb.200412022/DC1.

We thank T. Kaneko, T. Kouno, and K. Tatsumi for technical assistance. We also thank F. Kaji for his help in EM study; A. Kuma for technical guidance in caesarean delivery; K. Tateishi and H. Uozaki for discussion of liver pathology; and T. Fujimura and K. Murayama for amino acid measurements.

This work was supported in part by Grants-in-Aid from the Ministry of Education, Culture, Sports, Science and Technology of Japan.

Submitted: 3 December 2004
Accepted: 22 March 2005

References

Baumeister, W., J. Walz, F. Zuhl, and E. Seemuller. 1998. The proteasome: paradigm of a self-compartmentalizing protease. *Cell.* 92:367–380.

Bence, N.F., R.M. Sampat, and R.R. Kopito. 2001. Impairment of the ubiquitin-proteasome system by protein aggregation. *Science.* 292:1552–1555.

Bursch, W. 2001. The autophagosomal-lysosomal compartment in programmed cell death. *Cell Death Differ.* 8:569–581.

Ciechanover, A., and P. Brundin. 2003. The ubiquitin proteasome system in neurodegenerative diseases: sometimes the chicken, sometimes the egg. *Neuron.* 40:427–446.

Dunn, W.A., Jr. 1994. Autophagy and related mechanisms of lysosome-mediated protein degradation. *Trends Cell Biol.* 4:139–143.

Goldberg, A.L. 2003. Protein degradation and protection against misfolded or damaged proteins. *Nature.* 426:895–899.

Gronostajski, R.M., and A.B. Pardee. 1984. Protein degradation in 3T3 cells and tumorigenic transformed 3T3 cells. *J. Cell. Physiol.* 119:127–132.

Hanaoka, H., T. Noda, Y. Shirano, T. Kato, H. Hayashi, D. Shibata, S. Tabata, and Y. Ohsumi. 2002. Leaf senescence and starvation-induced chlorosis are accelerated by the disruption of an *Arabidopsis* autophagy gene. *Plant Physiol.* 129:1181–1193.

Ichimura, Y., T. Kirisako, T. Takao, Y. Satomi, Y. Shimonishi, N. Ishihara, N. Mizushima, I. Tanida, E. Kominami, M. Ohsumi, et al. 2000. A ubiquitin-like system mediates protein lipidation. *Nature.* 408:488–492.

Kabeya, Y., N. Mizushima, T. Ueno, A. Yamamoto, T. Kirisako, T. Noda, E. Kominami, Y. Ohsumi, and T. Yoshimori. 2000. LC3, a mammalian homologue of yeast Apg8p, is localized in autophagosome membranes after processing. *EMBO J.* 19:5720–5728.

Kabeya, Y., N. Mizushima, A. Yamamoto, S. Oshitani-Okamoto, Y. Ohsumi, and T. Yoshimori. 2004. LC3, GABARAP and GATE16 localize to autophagosomal membrane depending on form-II formation. *J. Cell Sci.* 117:2805–2812.

Klionsky, D.J., and S.D. Emr. 2000. Autophagy as a regulated pathway of cellular degradation. *Science.* 290:1717–1721.

Komatsu, M., I. Tanida, T. Ueno, M. Ohsumi, Y. Ohsumi, and E. Kominami. 2001. The C-terminal region of an Apg7p/Cvt2p is required for homodimerization and is essential for its E1 activity and E1-E2 complex formation. *J. Biol. Chem.* 276:9846–9854.

Kopito, R.R. 2000. Aggresomes, inclusion bodies and protein aggregation. *Trends Cell Biol.* 10:524–530.

Kuhn, R., F. Schwenk, M. Aguet, and K. Rajewsky. 1995. Inducible gene targeting in mice. *Science.* 269:1427–1429.

Kuma, A., M. Hatano, M. Matsui, A. Yamamoto, H. Nakaya, T. Yoshimori, Y. Ohsumi, T. Tokuhisa, and N. Mizushima. 2004. The role of autophagy during the early neonatal starvation period. *Nature.* 432:1032–1036.

Levine, B., and D.J. Klionsky. 2004. Development by self-digestion: molecular mechanisms and biological functions of autophagy. *Dev. Cell.* 6:463–477.

Lewandoski, M., K.M. Wassarman, and G.R. Martin. 1997. Zp3-cre, a transgenic mouse line for the activation or inactivation of loxP-flanked target genes specifically in the female germ line. *Curr. Biol.* 7:148–151.

Liang, X.H., S. Jackson, M. Seaman, K. Brown, B. Kempkes, H. Hibshoosh, and B. Levine. 1999. Induction of autophagy and inhibition of tumorigenesis by beclin 1. *Nature.* 402:672–676.

Massey, A., R. Kiffin, and A.M. Cuervo. 2004. Pathophysiology of chaperone-mediated autophagy. *Int. J. Biochem. Cell Biol.* 36:2420–2434.

Mizushima, N., T. Noda, T. Yoshimori, Y. Tanaka, T. Ishii, M.D. George, D.J. Klionsky, M. Ohsumi, and Y. Ohsumi. 1998. A protein conjugation system essential for autophagy. *Nature.* 395:395–398.

Mizushima, N., A. Yamamoto, M. Hatano, Y. Kobayashi, Y. Kabeya, K. Suzuki, T. Tokuhisa, Y. Ohsumi, and T. Yoshimori. 2001. Dissection of autophagosome formation using Apg5-deficient mouse embryonic stem cells. *J. Cell Biol.* 152:657–668.

Mizushima, N., Y. Ohsumi, and T. Yoshimori. 2002. Autophagosome formation in mammalian cells. *Cell Struct. Funct.* 27:421–429.

Mizushima, N., A. Yamamoto, M. Matsui, T. Yoshimori, and Y. Ohsumi. 2004. In vivo analysis of autophagy in response to nutrient starvation using transgenic mice expressing a fluorescent autophagosome marker. *Mol. Biol. Cell.* 15:1101–1111.

Mortimore, G.E., and A.R. Poso. 1987. Intracellular protein catabolism and its control during nutrient deprivation and supply. *Annu. Rev. Nutr.* 7:539–564.

Murata, S., H. Udono, N. Tanahashi, N. Hamada, K. Watanabe, K. Adachi, T. Yamano, K. Yui, N. Kobayashi, M. Kasahara, et al. 2001. Immunoproteasome assembly and antigen presentation in mice lacking both PA28alpha and PA28beta. *EMBO J.* 20:5898–5907.

Nakagawa, I., A. Amano, N. Mizushima, A. Yamamoto, H. Yamaguchi, T. Kamimoto, A. Nara, J. Funao, M. Nakata, K. Tsuda, et al. 2004. Autophagy defends cells against invading group *A Streptococcus*. *Science.* 306:1037–1040.

Nishino, I., J. Fu, K. Tanji, T. Yamada, S. Shimojo, T. Koori, M. Mora, J.E. Riggs, S.J. Oh, Y. Koga, et al. 2000. Primary LAMP-2 deficiency causes X-linked vacuolar cardiomyopathy and myopathy (Danon disease). *Nature.* 406:906–910.

Notterpek, L., M.C. Ryan, A.R. Tobler, and E.M. Shooter. 1999. PMP22 accumulation in aggresomes: implications for CMT1A pathology. *Neurobiol. Dis.* 6:450–460.

Ohsumi, Y. 2001. Molecular dissection of autophagy: two ubiquitin-like systems. *Nat. Rev. Mol. Cell Biol.* 2:211–216.

Perlmutter, D.H. 2002. Liver injury in alpha1-antitrypsin deficiency: an aggregated protein induces mitochondrial injury. *J. Clin. Invest.* 110:1579–1583.

Qu, X., J. Yu, G. Bhagat, N. Furuya, H. Hibshoosh, A. Troxel, J. Rosen, E.L. Eskelinen, N. Mizushima, Y. Ohsumi, et al. 2003. Promotion of tumorigenesis by heterozygous disruption of the beclin 1 autophagy gene. *J. Clin. Invest.* 112:1809–1820.

Seglen, P.O., and P. Bohley. 1992. Autophagy and other vacuolar protein degradation mechanisms. *Experientia.* 48:158–172.

Shintani, T., and D.J. Klionsky. 2004. Autophagy in health and disease: a double-edged sword. *Science.* 306:990–995.

Shintani, T., N. Mizushima, Y. Ogawa, A. Matsuura, T. Noda, and Y. Ohsumi. 1999. Apg10p, a novel protein-conjugating enzyme essential for autophagy in yeast. *EMBO J.* 18:5234–5241.

Sutovsky, P., R.D. Moreno, J. Ramalho-Santos, T. Dominko, C. Simerly, and G. Schatten. 1999. Ubiquitin tag for sperm mitochondria. *Nature.* 402:371–372.

Tanaka, Y., G. Guhde, A. Suter, E.L. Eskelinen, D. Hartmann, R. Lullmann-Rauch, P.M. Janssen, J. Blanz, K. von Figura, and P. Saftig. 2000. Accumulation of autophagic vacuoles and cardiomyopathy in LAMP-2-deficient mice. *Nature.* 406:902–906.

Tanida, I., N. Mizushima, M. Kiyooka, M. Ohsumi, T. Ueno, Y. Ohsumi, and E. Kominami. 1999. Apg7p/Cvt2p: a novel protein-activating enzyme essential for autophagy. *Mol. Biol. Cell.* 10:1367–1379.

Tanida, I., E. Tanida-Miyake, T. Ueno, and E. Kominami. 2001. The human homolog of *Saccharomyces cerevisiae* Apg7p is a protein-activating enzyme for multiple substrates including human Apg12p, GATE-16, GABARAP, and MAP-LC3. *J. Biol. Chem.* 276:1701–1706.

Tateishi, K., M. Omata, K. Tanaka, and T. Chiba. 2001. The NEDD8 system is essential for cell cycle progression and morphogenetic pathway in mice. *J. Cell Biol.* 155:571–579.

Tsukada, M., and Y. Ohsumi. 1993. Isolation and characterization of autophagy-defective mutants of *Saccharomyces cerevisiae*. *FEBS Lett.* 333:169–174.

Ueno, T., S. Watanabe, M. Hirose, T. Namihisa, and E. Kominami. 1990. Phalloidin-induced accumulation of myosin in rat hepatocytes is caused by suppression of autolysosome formation. *Eur. J. Biochem.* 190:63–69.

Waguri, S., N. Sato, T. Watanabe, K. Ishidoh, E. Kominami, K. Sato, and Y. Uchiyama. 1995. Cysteine proteinases in GH4C1 cells, a rat pituitary tumor cell line, are secreted by the constitutive and regulated secretory pathways. *Eur. J. Cell Biol.* 67:308–318.

Xue, L., G.C. Fletcher, and A.M. Tolkovsky. 1999. Autophagy is activated by apoptotic signalling in sympathetic neurons: an alternative mechanism of death execution. *Mol. Cell. Neurosci.* 14:180–198.

Yue, Z., S. Jin, C. Yang, A.J. Levine, and N. Heintz. 2003. Beclin 1, an autophagy gene essential for early embryonic development, is a haploinsufficient tumor suppressor. *Proc. Natl. Acad. Sci. USA.* 100:15077–15082.

Acta Neurol Scand 2007: 116: 340–344 DOI: 10.1111/j.1600-0404.2007.00876.x

ACTA NEUROLOGICA
SCANDINAVICA

Constant blood flow reduction in premotor frontal lobe regions in ALS with dementia – a SPECT study with 3D-SSP

Ishikawa T, Morita M, Nakano I. Constant blood flow reduction in premotor frontal lobe regions in ALS with dementia – a SPECT study with 3D-SSP.
Acta Neurol Scand 2007: 116: 340–344.

Objectives – We investigated the regional cerebral blood flow in amyotrophic lateral sclerosis with dementia (ALS-D) patients, using single photon emission computed tomography (SPECT). *Materials and methods* – The ^{123}I-IMP SPECT data for 5 ALS-D and 16 ALS patients were analyzed using three-dimensional stereotactic surface projection (3D-SSP). *Results* – 3D-SSP demonstrated marked prefrontal hypoperfusion in all the five ALS-D cases and significant bilateral prefrontal hypoperfusion in group comparisons. *Conclusions* – This study revealed prefrontal hypoperfusion in ALS-D cases to be an obvious abnormality with scientific objectivity.

T. Ishikawa, M. Morita, I. Nakano

Division of Neurology, Department of Internal Medicine, Jichi Medical University, Tochigi, Japan

Key words: amyotrophic lateral sclerosis with dementia; premotor frontal lobe region; regional cerebral blood flow; single photon emission computed tomography; three-dimensional stereotactic surface projection

Mitsuya Morita, Division of Neurology, Department of Internal Medicine, Jichi Medical University, 3311-1 Yakushiji, Shimotsuke, Tochigi 329 0498, Japan
Tel.: +81 285 58 7352
Fax: +81 285 44 5118
e-mail: morita@jichi.ac.jp

Accepted for publication March 25, 2007

Introduction

Amyotrophic lateral sclerosis (ALS) is a degenerative disorder that involves progressive muscle weakness, and the lesions are essentially restricted to upper and lower motor neurons. Traditionally, patients with ALS have been recognized to be free from cognitive impairment. Evidence is emerging, however, that the cognitive function is impaired in some ALS patients, and such cases have been repeatedly described, especially in Japan (1).

Single photon emission computed tomography (SPECT) studies have been performed for the evaluation of the regional cerebral blood flow (rCBF) in various neurodegenerative disorders, including ALS and ALS-D. Such studies revealed cortical hypoperfusion in the premotor frontal lobe cortex and/or motor cortex in ALS (2, 3) or ALS with dementia (ALS-D) (4, 5), leading the researchers to state that ALS-D is included in the spectrum of ALS (6). The reported hypoperfusion in these regions, however, lacked objectivity, because the SPECT data were not standardized. With recent advances in computer-assisted analysis of SPECT images using three-dimensional stereotactic surface projection (3D-SSP) (7, 8), we have become able to detect a slight change in rCBF with scientific objectivity. Nevertheless, there have been few studies to discriminate subjects with ALS-D from non-demented ALS cases using such statistical methods. The purpose of this study was to evaluate rCBF in ALS-D and ALS cases using an objective and accurate method for analysis such as 3D-SSP, and to discuss the relationship between ALS-D and classic ALS.

Material and methods

Cases

Forty-one ALS cases had been diagnosed in the Neurology Department of Jichi Medical University from 1997 to 2003, five of whom had dementia. Among them, 16 ALS patients and five ALS with dementia patients could be evaluated by SPECT. Five ALS-D (two men and three women, mean ± SD: 54.8 ± 3.4 years old) and 16 ALS cases (nine men and seven women, mean ± SD: 66.5 ± 11.8 years old) were selected for analysis. The diagnosis of ALS was established according to the El Escorial criteria (9). None of the patients had either symptoms of a cerebrovascular disease or infarcts detectable in CT or MR images.

Table 1 Clinical features of the amyotrophic lateral sclerosis with dementia (ALS-D)

ALS-D cases	Age (years old) /Sex	The duration of illness at the time of SPECT (months)	Initial symptom	HDS-R	WAIS-R	Loss of memory	Insight into disease	Personality change /Emotional disorder	Autopsy
ALS-D 1	58/F	8	Memory loss	19	N/A	+	−	+	−
ALS-D 2	50/M	8	Memory loss	N/A	Verbal (57) Performance (51) Full (47)	+	−	+	+
ALS-D 3	59/F	19	Upper limb weakness	22	Verbal (100) Performance (75) Full (89)	−	−	+	+
ALS-D 4	52/F	27	Paranoia	18	N/A	+	−	+	+
ALS-D 5	55/M	45	Personality change	19	N/A	+	−	+	−
	54.8 ± 3.4 (mean ± SD)	21.4 ± 13.8 (mean ± SD)							
ALS cases									
Total 16 cases	66.5 ± 11.8 (mean ± SD)	21.4 ± 14.7 (mean ± SD)							

When individuals exhibited both ALS and an intellectual impairment constellation, such as loss of memory, personality change, emotional disorder and language impairment (the clinical features are summarized in Table 1), the diagnosis of ALS-D was made. For the evaluation of intellectual impairment, we used the Wechsler Adult Intelligence Scale-Revised (WAIS-R) and/or the revised Hasegawa Dementia Scale (HDS-R). The HDS-R is widely used as a brief cognitive screen instrument in Japan, and the result is known to be correlated well with the Mini-Mental State Examination (MMSE). The low-normal cut off is estimated to be 20, and the results are summarized in Table 1. Two ALS-D cases were also evaluated with the WAIS-R.

Assessment with the WAIS-R yielded a verbal IQ of 57, performance IQ of 51 and full IQ of 47 in case 2, a verbal IQ of 100, performance IQ of 75 and full IQ of 89 in case 3. Case 3 developed limb weakness as an initial symptom, and her intellectual impairment was negligible when she was diagnosed as having ALS, and SPECT study was carried out. Thereafter, she developed prominent dementia.

All the five ALS-D cases finally died of respiratory failure because of motor neuron involvement. Autopsy was performed in three cases (case 2, 3, and 4), and the diagnosis of ALS-D was confirmed according to the result of the autopsy. A total of 33 healthy volunteers (21 men and 12 women, mean ± SD: 58.6 ± 11.0 years old) was used as normal control subjects for 3D-SSP analysis.

SPECT and 3D-SSP

Single photon emission computed tomography with [^{123}I] isopropyl amphetamine (^{123}I-IMP SPECT) image sets was performed. The duration of illness at the time of SPECT was 21.4 ± 13.8 (mean ± SD) months in the ALS-D group and 21.4 ± 14.7 (mean ± SD) months in the ALS one, respectively. We performed 3D-SSP using the Neurological Statistical Image Analysis Software (NEUROSTAT) to evaluate the spatial distribution of an abnormal CBF, (8) and iSSP 35 for Windows to produce single subject *Z*-maps of decreased perfusion in patients. Following stereotactic anatomic standardization, the CBF in an individual's SPECT image set was extracted as a set of predefined surface pixels, which was used in the subsequent analysis. To quantify perfusion deficits, the normalized CBF in each patient was compared with that in 33 normal controls by pixel-by-pixel *Z*-score analysis ([normal mean]-[individual value])/(normal standard deviation; SD). We also compared the intergroup differences between the ALS-D group and normal controls, the ALS-D and ALS groups, and the ALS group and normal controls. A positive *Z*-score represents a reduced CBF in a patient relative to the control mean. In this study, we considered that a *Z*-score of > 3.0 was significant.

Results

The statistical *Z*-scores obtained with 3D-SSP in the ALS-D patients are presented in the Fig. 1.

The reduction of rCBF was consistently prominent and widespread in the middle to inferior areas of the premotor frontal lobe in all five ALS-D patients, while the rCBF decrease in such regions was only subtle and patchy in ALS patients. A mild decrease in the unilateral temporal lobe was also seen in all the five ALS-D patients.

A significant rCBF reduction in the bilateral frontal lobes, especially the premotor frontal lobes,

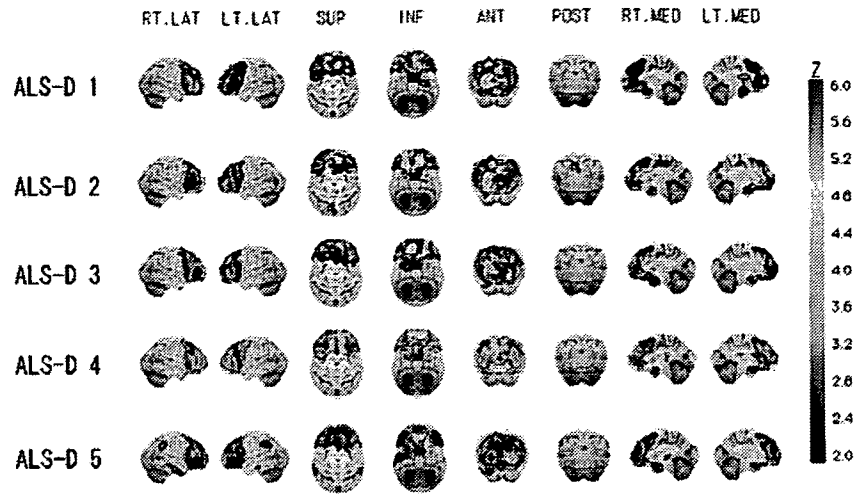

Figure 1. Three-dimensional stereotactic surface projection (3D-SSP) of the amyotrophic lateral sclerosis with dementia (ALS-D) cases compared with normal controls. The *Z*-score images obtained with 3D-SSP demonstrated marked regional cerebral blood flow reduction in the bilateral frontal lobes, especially the prefrontal lobes, in all five ALS-D patients. Images are constructed from eight views [in each line, from left to right, right lateral (RT. LAT), left lateral (LT. LAT), superior (SUP), inferior (INF), anterior (ANT), posterior (POST), right medial (RT. MED), and left medial (LT. MED)].

was evident in the ALS-D group compared with not only in normal controls but also in the ALS group (Fig. 2). One part of the left temporal lobe, the parahippocampal gyrus, also exhibited subtle hypoperfusion in the ALS-D group. On the contrary, in the ALS group, there were subtle rCBF decreases in the anterior part of the cingulate gyrus and the posterior part of the corpus callosum compared with in normal controls. Neither the ALS-D group nor the ALS one exhibited an obvious rCBF reduction in the regions corresponding to the precentral gyrus.

Discussion

Scintigraphical studies have been performed for the evaluation of rCBF in various neurodegenerative disorders, and some researchers have reported cortical hypoperfusion in the frontal cortex and motor cortex in ALS-D (4, 5). In the previous reports, however, as subjective approaches such as visual inspection were used, the reported hypoperfusion in these regions lacked objectivity. The 3D-SSP we used in this study is far superior to the visual inspection method in terms of objectivity. In addition, its sensitivity is reported to be high enough to be able to discriminate patients with a very early stage of the Alzheimer disease from healthy controls (7).

In our study, cortical hypoperfusion in the frontal lobe in the ALS-D group was consistently prominent compared to in the ALS cases, although the mean age of the ALS-D cases was lower than that of the controls or the ALS cases. CBF tends

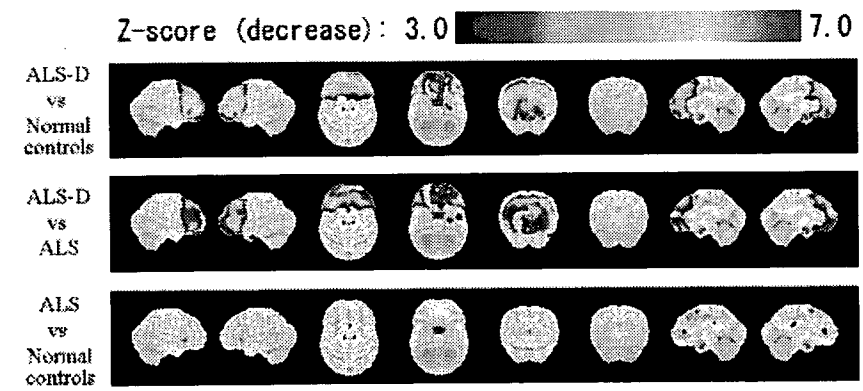

Figure 2. Decrease of regional cerebral blood flow (rCBF) adjusted to the global mean cerebral blood flow using three-dimensional stereotactic surface projection (3D-SSP) in group comparisons. 3D-SSP demonstrated a significant rCBF reduction in the bilateral frontal lobes, especially the prefrontal lobes, in the amyotrophic lateral sclerosis with dementia (ALS-D) group, when compared with either in normal controls or in the ALS group. On the contrary, subtle rCBF decreases in the anterior part of the cingulate gyrus and the posterior part of the corpus callosum were seen in the ALS group when compared with in normal controls. Images are constructed from 8 views in the same order as Fig. 1.

to be decreased in aged persons, so we might have underestimated the decrease in rCBF in the ALS-D group.

The change observed was notable in the inferolateral premotor frontal cortex in 4 of the 5 ALS cases, this being consistent with the previous results on ^{123}I-IMP SPECT and visual inspection (4, 5). This result is also supported by a previous neuropathological study on ALS-D that showed involvement of the inferomedial premotor frontal cortex, which is known to play important roles in emotional control and intellectual function (10). Thus, the decreased rCBF in the bilateral frontal lobe may play a role in the cognitive dysfunction in this condition.

In some of our ALS patients, a subtle reduction of rCBF in some parts of the frontal lobes, but strangely not in the precentral motor cortex, was observed, but the region was relatively restricted and variable. Our results are contrary to the findings in some previous studies (2, 3, 5) that revealed bilateral frontal hypoperfusion in ALS on visual inspection. In this study, no rCBF reduction was seen in the bilateral motor cortices not only in ALS-D but also in ALS. This result might indicate that there is actually no rCBF reduction in ALS, or we also need to consider the limit of sensitivity of this method.

What should we think about the relation between ALS and ALS-D? Most ALS-D cases reported previously shared characteristic neuropathological findings such as motor neuronal degeneration and Bunina bodies with classic/sporadic ALS. From the standpoint that ALS is a disease with widespread involvement of not only the pyramidal tract but also other systems, ALS-D belongs to the same clinical entity as ALS. However, the pattern of rCBF reduction in the ALS-D group in this study is apparently different from that of ALS, the pattern of ALS-D resembling that of fronto-temporal dementia (FTD). The hyporperfusion in the ALS-D group in this study could lead us to think that ALS-D is one form of FTD. However, most ALS-D cases reported previously had characteristic neuropathological findings consistent with sporadic ALS, such as Bunina bodies. It is essential that ALS-D is defined by supporting neuropathological investigation. If dementia is ultimately superimposed on ALS, the same decreasing rCBF pattern as in ALS-D should be observed in ALS cases, especially in ones with a long history. Actually, the most prominent rCBF reduction was observed in the case with the longest duration of the disease (45 months) among the ALS-D cases (case 5 of ALS-D). However, none of the 16 ALS cases showed the same pattern as that in ALS-D.

Furthermore, it is interesting that the cortical hypoperfusion in the frontal lobe was observed in one ALS-D case before the development of dementia. Case 3 with ALS-D developed limb weakness as an initial symptom, and at 19 months after the onset, ^{123}I-IMP SPECT was performed. Although the reduction of rCBF in the frontal lobe was obvious, her intellectual impairment was negligible at that time and became markedly worse after the examination. This suggests that a reduction of frontal rCBF could precede clinically evident dementia.

Based on our 3D-SSP analysis, it is reasonable to suppose that the pathogenesis of ALS-D is different from that of ALS, and 3D-SSP analysis might have a high predictive value for the diagnosis of ALS-D even at the stage of cryptic dementia.

There is the possibility that ALS-D may be overlooked, because ALS patients with severe bulbar symptoms tend to have trouble in verbal communication. We should always consider possible dementia hidden behind ALS, and recommend a SPECT study for ALS patients with any subtle signs and symptoms suggesting dementia.

Conclusion

Using 3D-SSP, we have demonstrated that ALS-D patients have a significantly reduced rCBF in the bilateral premotor frontal lobes compared with controls and ALS patients. The present study indicated that SPECT with 3D-SSP can clearly and objectively distinguish ALS-D from ALS. This finding seems to be useful for the diagnosis of ALS-D even at an early stage of dementia. A decreased rCBF in the bilateral premotor frontal lobes may be associated with dementia in ALS-D patients and help us to recognize the pathogenesis of the disease.

Acknowledgements

The authors are very grateful to Mr Y. Kawamura for providing the cases for the SPECT database, and to Mr M. Suzuki for the skilful editing.

References

1. Mitsuyama Y. Presenile dementia with motor neuron disease in Japan: clinico-pathological review of 26 cases. J Neurol Neurosurg Psychiatry 1984;**47**:953–9.
2. Abe K, Fujimura H. Single-photon emission computed tomographic investigation of patients with motor neuron disease. Neurology 1993;**43**:1569–73.
3. Waldemar G, Vorstrup S. Focal reductions of cerebral blood flow in amyotrophic lateral sclerosis: a [^{99m}Tc]-*d,l*-HMPAO SPECT study. J Neurol Sci 1992;**107**:19–28.

4. Neary D, Snowden JS. Frontal lobe dementia and motor neuron disease. J Neurol Neurosurg Psychiatry 1990;**53**: 23–32.
5. Vercelletto M, Ronin M. Frontal type dementia preceding amyotrophic lateral sclerosis: a neuropsychological and SPECT study of five clinical cases. Eur J Neurol 1999;**6**:295–9.
6. Talbot PR, Goulding PJ. Inter-relation between 'classic' motor neuron disease and frontotemporal dementia: neuropsychological and single photon emission computed tomography study. J Neurol Neurosurg Psychiatry 1995;**58**:541–7.
7. Imabayashi E, Matsuda H. Superiority of 3-dimensional stereotactic surface projection analysis over visual inspection in discrimination of patients with very early Alzheimer's disease from controls using brain perfusion SPECT. J Nucl Med 2004;**45**:1450–7.
8. Minoshima S, Frey KA. A diagnostic approach in Alzheimer's disease using three-dimensional stereotactic surface projections of fluorine-18-FDG PET. J Nucl Med 1995;**36**: 1238–48.
9. Brooks BR. El Escorial World Federation of Neurology criteria for the diagnosis of amyotrophic lateral sclerosis. Subcommittee on Motor Neuron Diseases/Amyotrophic Lateral Sclerosis of the World Federation of Neurology Research Group on Neuromuscular Diseases and the El Escorial 'Clinical limits of amyotrophic lateral sclerosis' workshop contributors. J Neurol Sci 1994;**124**:(Suppl.): 96–107.
10. Abe K, Fujimura H. Cognitive function in amyotrophic lateral sclerosis. J Neurol Sci 1997;**148**:95–100.

■特集　クロストーク：「神経心理学」と「神経病理学」

痴呆を伴う筋萎縮性側索硬化症の病理

中野今治

要旨：痴呆を伴う筋萎縮性側索硬化症患者は，性格変化・異常言動などの精神症状を呈する．精神症状が運動ニューロン症候に先行する場合が多い．生命予後は下位運動ニューロン症候の出現に懸かっている．神経病理学的には，大脳皮質病変と運動ニューロン病変に大別できる．前者は通常側頭葉に優位であり，側頭葉極内側皮質，海馬足CA1-支脚，迂回回，扁桃核に変性が高頻度に見られる．これのみでは痴呆を説明するのは困難であるが，この病変が大脳病変の初発部位である可能性がある．海馬歯状回顆粒細胞や海馬傍回等の小ニューロンにubiquitin陽性封入体が出現する．黒質にも高頻度に変性が見られる．運動ニューロン病変は古典型ALSと酷似しているが，Bunina小体が目立ち，上位運動ニューロン障害が軽い傾向を示す．最近は上位運動ニューロン障害が優位のALSDも報告され，さらには下位運動ニューロン障害もBunina小体も認められないもののALSDと酷似した大脳病変を示す上位運動ニューロン障害優位の症例群も報告されている．

神経心理学　22；171-177，2006

Key words：痴呆を伴う筋萎縮性側索硬化症，神経病理，側頭葉病変，CA1-支脚移行部病変，ユビキチン化封入体
amyotrophic lateral sclerosis, neuropathology, temporal lobe change, CA1-subiculum transitional zone lesion, ubiquitinated inclusion

はじめに

古典型筋萎縮性側索硬化症（古典型ALS：Charcot病）は上位下位運動ニューロン症候を呈するものの知的異常は呈さない．これに対し，ALS症候と独特の痴呆を呈するグループが存在し，痴呆を伴うALS（ALS with dementia：ALSDと略す）と呼ばれる．ただし，ALSDが古典型ALS（Charcot病）の範疇に入るのか，あるいはこれとは独立した疾患単位なのかについての結論は得られていない．

ALSDの最初の剖検報告は1929年のMeyerのものと思われる[7]．1961年にvan Reethらが報告した1例[18]は，Bunina小体を初めて記載したことで特筆される（原著[18] Fig. 20）．その後，ALSDは主として本邦において注目を集め，報告されてきた．その端緒となったのは1964年，湯浅の臨床報告例である[21]．本邦での最初の剖検報告は1966年，日本神経病理学会でなされた．

1994年，主要病変が前頭葉と側頭葉に存在して，アルツハイマー病とは異なる臨床病理像を呈する疾患群を包括する概念として，前頭側頭型痴呆（FTD）が提唱された[16]．ALSDもこの中に包含され，運動ニューロン型前頭側頭型痴呆（MND-FTD）と呼ばれている[9]．

臨床像

ALSDの発症年齢は38～77歳，平均56歳，男女比は約2：1である．その症状は精神症状と運動ニューロン症状に大別できるが，多くは精神症状が先行する[12]．生命予後を決定するのは下位運動ニューロン症候であり，精神症状が先行して

Neuropathology of amyotrophic lateral sclerosis with dementia
自治医科大学神経内科，Imaharu Nakano：Division of Neurology, Department of Medicine, Jichi Medical University
別刷請求先：〒329-0498　河内郡南河内町薬師寺3311-1　自治医大神経内科　中野今治
inakano@ms2.jichi.ac.jp

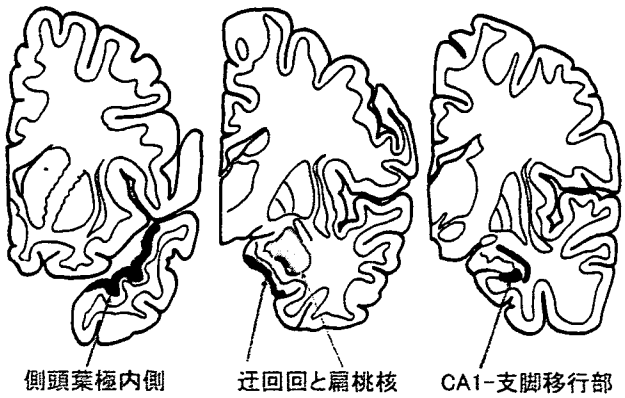

図5 痴呆を伴うALSの側頭葉病変

トログリアの増生，ニューロピルの粗鬆化が認められるが，側副溝を越えて外側皮質に入ると変化は軽くなるかほとんど見られなくなる．

図5に側頭葉で見られる病変部位を図示してある．

2) ubiquitin化封入体

これはALSDの海馬歯状回顆粒細胞，内嗅野，側頭葉皮質，前頭葉皮質の小ニューロンにおいて認められる細胞質内封入体で，抗ユビキチン抗体で陽性に染色されるが，抗ニューロフィラメント抗体や抗タウ蛋白抗体では染まらない[14]．また，パラフィン包埋した光学顕微鏡用標本では，いずれの染色に於いてもこの封入体は同定できない．ただ，海馬歯状回顆粒細胞のエポン包埋した準超薄切片でよく目をこらせば楕円形の封入体が同定できる．ただ，抗ユビキチン抗体免疫染色でも，この封入体の数はさほど多くなく，ぱらぱらと散在するとの印象を受ける程度である．海馬歯状回顆粒細胞で見られる場合には，円形から楕円形の明瞭なubiquitin陽性封入体として観察される(図6)．電顕的には限界膜を有さず，不明瞭な線維状構造と電子密度の高い不規則な顆粒との混交物である（図7)．抗ユビキチン抗体での免疫電顕では，この線維状の構造と顆粒とが陽性に染まっている．

ところで，ALSDでは歯状回顆粒細胞の脱落はなく，ubiquitin化した封入体を含む顆粒細胞にも封入体以外の変性所見は見られない．大脳皮質の変性に関してこの封入体の有する意義は今後

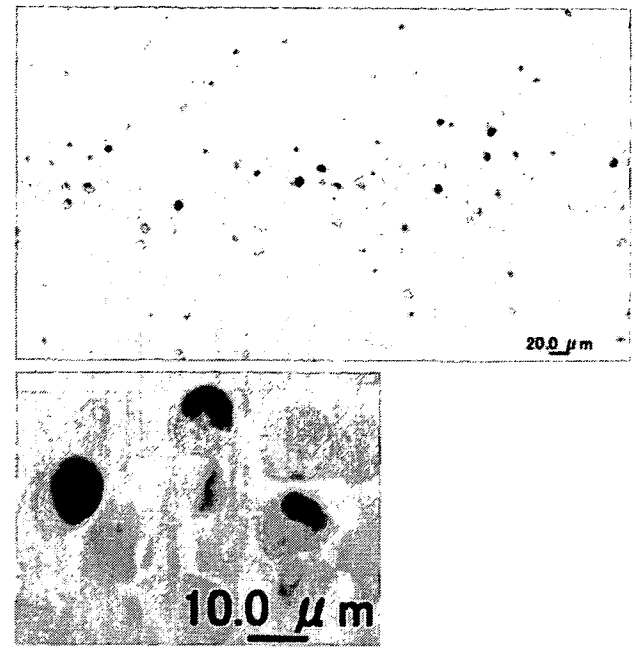

図6 図1例の海馬顆粒細胞に見られるユビキチン陽性封入体．抗ユビキチン抗体免疫染色

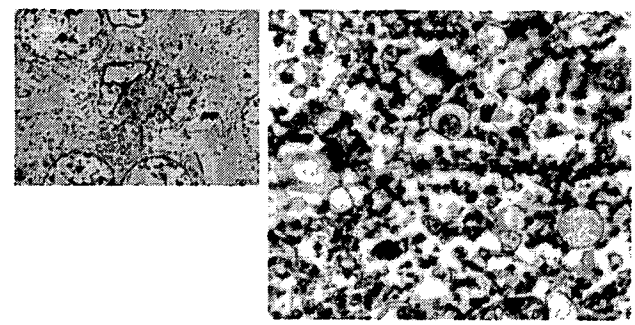

図7 ALSD海馬歯状回顆粒細胞のユビキチン陽性封入体の電顕像（左：矢印で囲まれている)．右：左図の封入体の強拡大．顆粒と少数の線維構造から形成されている．左：約3,000×，右：約10,000×

の研究に待たねばならない．

3) 痴呆のないALSに見られる側頭葉病変

痴呆のないALSでもALSDと同じ側頭葉病変を呈する場合があり（図8，9)[9][10]，その際大脳皮質ニューロン，とくに歯状回顆粒細胞にubiquitin化した封入体がみられる．これらの症例が，真に痴呆を呈さなかったのか，あるいは球症状の合併により，痴呆が見逃されたのか，その決定は今後の課題である．

2．運動ニューロン病変：運動ニューロンは古典型ALSと同質の病変を呈する．Bunina小体は

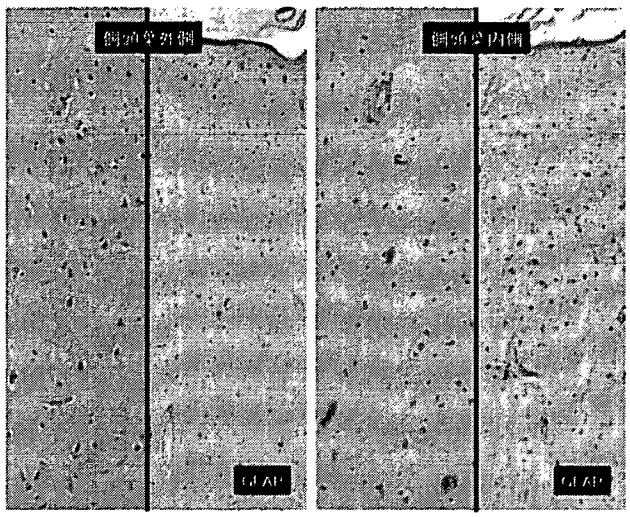

図8 “痴呆が認められなかった”ALSの側頭葉極皮質浅層．内側面の変性とグリオーシスが明らかである．

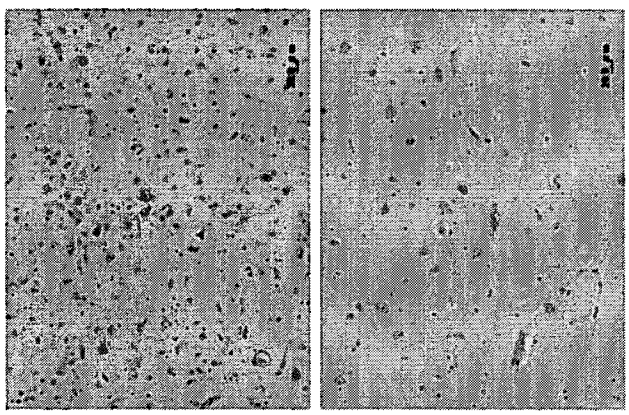

図9 “痴呆の認められなかった”ALSの海馬．CA1自体（右）は良く保たれているのに対して，CA1-支脚移行部（左）には明らかなニューロン脱落とグリオーシスが見られる．HE，20×．

古典型ALSで見られるものよりも大型で，数珠状に連なり多数かつより広範囲に出現する傾向がある[11]．Bunina小体が最初にALSDで記載された[18]のも偶然ではないかもしれない．錐体路変性は一般に軽度だが，鍍銀染色で大径線維の数の減少が確認できる．また，中心前回のBetz巨細胞も脱落している．

3．その他の病変

通常はLewy小体を伴わない黒質の変性が高頻度に認められる[20]．

側頭葉病変の意義とALSDの位置づけ

側頭葉の皮質病変は，前頭・頭頂葉に病変が明らかでない例でも認められ，この部位がALSDの大脳皮質病変の初発部位である可能性がある．しかし，この病変のみでALSDの精神症状が説明可能か否かは未確定であり，今後の検討が必要である．

側頭葉の萎縮が高度で葉性萎縮と呼ぶにふさわしいALSD例があることも確かであり，ALSDをPick病との関連で捉えようとの立場にも一理ある．しかし，Pick病とALSの合併として報告された例はいずれもPick嗜銀球を欠いている．Pick嗜銀球とBunina小体を含むようなALSD例が報告されるまでは，ALSDはPick病と異なる疾患として捉えた方が混乱が少ないと思われる．

ALSDに絡む最近の動き

1．Motor Neuron Disease-Inclusion Dementia（MNDID）：1996年，Jackson Mらは，臨床的には前頭側頭方痴呆を呈し，運動ニューロン症候を欠き，神経病理学的にはユビキチン陽性封入体を初めとしてALSDと区別できない病変を呈するものの運動ニューロン病変を示さない症例群を報告した[5]．ここで見られるユビキチン陽性封入体を彼らはALSDで見られるものと同一視して，motor neuron disease-inclusion（MNDI）と呼び，これらの疾患群をMNDIDと命名した[5]．しかしながら，彼らの症例では脊髄が採取されておらず，彼ら自身1996年の論文で「我々の症例がもっと長く生きていれば，運動ニューロン症候を呈した可能性がある」と推測している．実際，そのようなことを示す症例が次々に報告されており[2][17]，MNDIDはALSDの不全型であるとの考え方が一般的である．

2．上位運動ニューロン優位の障害を示す前頭側頭型痴呆

ALSDでは，下位運動ニューロン症候が優位であり，上位運動ニューロン症候は目立たない．ところが，近年，初期には原発性側索硬化症と診

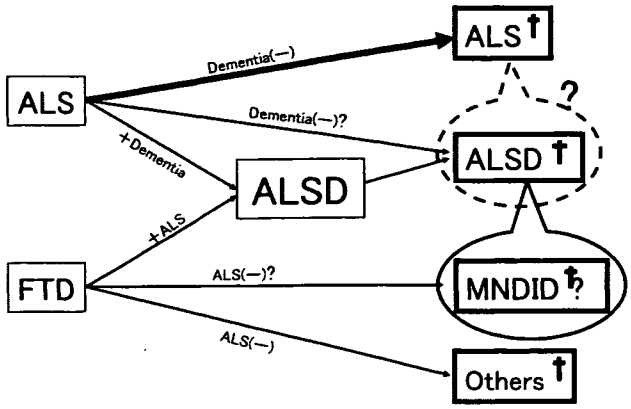

図10 ALS, ALSD, FTD, MNDIDの相関

断されるほどの上位運動ニューロン症候と痴呆を呈し，剖検してみると大脳皮質ニューロンにユビキチン陽性封入体と海馬CA1−支脚移行部の限局変性があり，軽度ではあるが下位運動ニューロンの変性とBunina小体も認められる症例の報告が本邦から相次いでなされている[6) 13) 19)]．

現時点では，これらの疾患群もALSDの範疇に含めて議論した方が良さそうである．

3. Pick嗜銀球の無い葉性萎縮とALSD

葉性萎縮を呈する疾患には，Pick嗜銀球を伴う群と伴わない群があり，前者のみがピック病あるいはピック小体病と呼ばれる傾向にある．そうすると後者の位置づけが問題となる．

Pick嗜銀球の無い葉性萎縮では，1. 大脳では，前頭・側頭葉皮質の萎縮と変性，motor neuron-disease inclusionおよびCA1−支脚移行部の限局変性が見られ，2. 運動ニューロンでは，錐体路変性は見られるものの下位運動ニューロンの変性は無いか在っても軽度であり，さらにはBunina小体が見られない，という特徴を有する[3) 4)]．

Pick嗜銀球の無い葉性萎縮では，大脳病変のみを見れば上位運動ニューロン障害優位のALSDと変わるところが無いように見える．下位運動ニューロン病変，特にBunina小体が見られないとされる点が異なる点であるが，病理組織学的に或る構造が在ることを示すのは比較的容易であるが，無いことを証明するのは至難である．Pick嗜銀球の無い葉性萎縮においてBunina小体が無いと断言することはできないであろうし，さらにはBunina小体や下位運動ニューロン変性が出現する前に死亡した可能性（上位運動ニューロン障害優位のALSDの不全型）を否定できないであろう．この問題の解決には症例の蓄積と時間を懸けての検討が必用のように思われる．

図10にALS, ALSD, FTD, MNDIDの推測される相関を示しておく．Pick嗜銀球の無い葉性萎縮群が何処に位置するかは今後の課題である．

文 献

1) Brun A, Englund B, Gustafson L et al : Clinical and neuropathological criteria for frontotemporal dementia. J Neurol Neurosurg Psychiatry, 67 : 416-418, 1994
2) Holton JL, Revesz T, Crooks R et al : Evidence for pathological involvement of the spinal cord in motor neuron disease-inclusion dementia. Acta Neuropathol, 103 : 221-227, 2002
3) 池田研二，土谷邦秋，秋山治彦ら：ピック病の再検討—“ピック小体を伴わない葉性萎縮”の位置づけ—．神経進歩 45 : 329-341, 2001
4) Ikeda K, Tsuchiya K : Motor neuron disease group accompanied by inclusions of unidentified protein signaled by ubiquitin. Neuropathology, 24 : 117-124, 2004
5) Jackson M, Lennox G, Lowe J : Motor neuron disease-inclusion dementia. Neurodegeneration, 5 : 339-350, 1996
6) 小長谷正明，酒井素子，飯田光男ら：著明な錐体路障害と前・側頭葉萎縮を呈した運動ニューロン疾患の1剖検例—特に原発性側索硬化症との関連について—．臨床神経 35 : 384-390, 1995
7) Meyer A : Uber eine der amyotrophischen Lateralsklerose nahestehende Erkrankung mit psychischen Storungen. Zugleich ein Beitrag zur Frage der spastischen Pseudosklerose (A. Jakob). Z Gesamte Neurol Psychiatr, 121 ; 107-128, 1929
8) Mitsuyama Y, Kogoh H, Ata K : Progressive dementia with motor neuron disease. Eur Arch Psychiatry Neurol Sci, 235 : 1-8, 1985
9) Nakano I : Frontotemporal dementia with motor neuron disease (ALS with dementia). Neuropathology, 20 : 68-75, 2000

10) Nakano I : Temporal lobe lesions in amyotrophic lateral sclerosis with or without dementia — a neuropathological study —. Neuropathology, 13 ; 215-227, 1993
11) Nakano I, Iwatsubo T, Hashizume Y et al : Bunina bodies in neurons of the medullary reticular formation in amyotrophic lateral sclerosis. Acta Neuropathol, 85 ; 471-474, 1993
12) 中野今治：ALSと痴呆．神経進歩 40 ; 63-74, 1996
13) 中山 宏，新井信隆，安藤 蒸：全経過18年で末期にALS病変をきたしたと思われるPick病の1剖検例．Neuropathol, 16 (Suppl.) ; 125, 1996
14) Okamoto K, Murakami N, Kusaka H et al : Ubiquitin-positive intraneuronal inclusions in the extramotor cortices of presenile dementia patients with motor neuron disease. J Neurol, 239 ; 426-430, 1992
15) 岡本幸市：痴呆を伴う筋萎縮性側索硬化症の海馬病変．脳神経 50 ; 915-922, 1998
16) The Lund and Manchester Groups : Clinical and neuropathological criteria for frontotemporal dementia. J Neurol Neurosurg Psychiatry, 57 ; 416-418, 1994
17) Toyoshima Y, Tan C-H, Kozakai T et al : Is motor neuron disease-inclusion dementia a forme fruste of amyotrophic lateral sclerosis with dementia? An autopsy case further supporting the disease concept. Neuropathology, 25 ; 214-219, 2005
18) Van Reeth PCh, Perier O, Coers C et al : Demence de Pick associee a une sclerose laterale amyotrophique atypique (Etude anatomoclinique). Acta Neurol Psychiatr Bel, 61 ; 309-325, 1961
19) 山崎峰雄，山崎昌子，森 修ら：精神症状，緩徐進行性失語で発症した上位運動ニューロン障害優位のALSの1剖検例—痴呆を伴うALSの1型か？—．Neuropathology, 20 (suppl.) ; 85, 2000
20) 吉田眞理，村上信之，橋詰良夫ら：痴呆を伴う運動ニューロン疾患13例の臨床病理学的検討．臨床神経 32 ; 1193-1202, 1993
21) 湯浅亮一：痴呆を伴う筋萎縮性側索硬化症について．臨床神経 4 ; 529-533, 1964

Neuropathology of amyotrophic lateral sclerosis with dementia

Imaharu Nakano

Division of Neurology, Department of Medicine, Jichi Medical University

Patients with amyotrophic lateral sclerosis with dementia (ALSD) show characteristic mental and behavioral changes, represented by lack of insight into their tragic condition. Psychiatric symptoms usually precede motor neuron symptoms, which determine the life prognosis of the patients. In this condition, the neuropathology is classified as cerebral pathology and motoneuron one. The former is usually emphasized and probably earliest observed in the medial side cortex of the temporal pole, border zone between the CA1 and subiculum, ambient gyrus and entorhinal area, and amygdala. Another finding unique to the cerebral pathology of ALSD is cytoplasmic ubiquitinated inclusion bodies in the dentate gyrus granular neurons and other cortical small neurons. Motoneuron pathology is almost the same as that in classic ALS except for a tendency for Bunina bodies to be more prominent and for the pyramidal tract to be less affected in this condition. The substantia nigra is more or less degenerated without Lewy bodies. A condition recently proposed as motor neuron disease-inclusion dementia seems to be a forme froste of ALSD. Several cases of ALSD with upper motor neuron-dominant involvement have been also reported, showing the possibility that extension of ALSD will be widened than considered so far.

(Japanese Journal of Neuropsychology 22 ; 171-177, 2006)